ACES School of Electromagnetics
Online Lectures
February 21, 2026

Microwave and Millimeter-wave Imaging in Real Time

Part 3: Fourier-domain Direct Image-reconstruction Methods

Natalia K. Nikolova
nikolova@ieee.org

McMaster University
Department of Electrical and Computer Engineering
Electromagnetic Vision (EMVi) Research Laboratory
Hamilton, ON CANADA

LECTURE OVERVIEW

Part 1: Introduction
- Applications of Microwave and mm-Wave Imaging (MMI)
- Components of MMI Systems
- Data Acquisition Systems, Antennas and Antenna Arrays in MMI

Part 2: Models of Electromagnetic Scattering
- Data and State Equations
- Linearized Scattering Models

Part 3: Fourier-domain Direct Image-reconstruction Methods
- Core Concept: Data Point-spread Function (PSF)
- Quantitative Microwave Holography (QMH)
- Scattered Power Mapping (SPM)

S-PARAMETER DATA EQUATION, REVISITED

$$\underbrace{S_{\zeta}^{\mathrm{sc}}(\mathbf{r},\omega)}_{\substack{\text{extracted data}\\ \zeta=(i,j)}} = \underbrace{\frac{\mathrm{i}\omega\varepsilon_0}{2a_i a_j}}_{\substack{\text{known}\\ \text{constant } \kappa_\zeta}} \iiint_{V_\mathrm{s}} \underbrace{\Delta\varepsilon_\mathrm{r}(\mathbf{r}')}_{\substack{\text{complex}\\ \text{permittivity}\\ \text{contrast}}} \underbrace{\mathbf{E}_{\zeta,\mathrm{Rx}}^{\mathrm{inc}}(\mathbf{r}',\mathbf{r};\omega)}_{\text{Green's vector function}} \cdot \underbrace{\mathbf{E}_{\zeta,\mathrm{Tx}}^{\mathrm{tot}}(\mathbf{r}',\mathbf{r};\omega;\Delta\varepsilon_\mathrm{r}(\mathbf{r}'))}_{\text{total internal field}} d\mathbf{r}'$$

contrast to be found
$\Delta\varepsilon_\mathrm{r}(\mathbf{r}') = \varepsilon_\mathrm{r}(\mathbf{r}') - \varepsilon_{\mathrm{r,b}}$

data space

$\zeta = 1,\ldots,N_\mathrm{T}\ (\sim 1 \text{ to } 10)$ response types
$n = 1,\ldots,N_\mathrm{S}\ (\sim 10^3 \text{ to } 10^4)$ spatial samples
$k = 1,\ldots,N_\omega\ (\sim 10^3)$ frequency samples

number of unknowns

number of voxels: $p = 1,\ldots,N_\mathrm{v}\ (\sim 10^4 \text{ to } 10^6)$
$\Delta\varepsilon_\mathrm{r}$ & $\mathbf{E}_{\zeta,\mathrm{Tx}}^{\mathrm{tot}}(\mathbf{r},\omega)$ to be found at each voxel

How can we solve a nonlinear problems with $>10^5$ unknows and $>10^6$ data points within seconds?

THE DIRECT (LINEAR) INVERSE-PROBLEM SOLUTION

1) linearize the problem with Born's approximation

replace $\mathbf{E}^{\text{tot}}_{\zeta,\text{Tx}}\left(\Delta\varepsilon_{\text{r}}(\mathbf{r}')\right)$ with incident-field distribution $\mathbf{E}^{\text{inc}}_{\zeta,\text{Tx}}(\mathbf{r}')$ which is independent of the unknown $\Delta\varepsilon_{\text{r}}(\mathbf{r}')$

measurement with antenna pair at $\mathbf{r}$

$$S^{\text{sc}}_{\zeta}(\mathbf{r},\omega) = \kappa_{\zeta}\iiint_{V_{\text{s}}} \Delta\varepsilon_{\text{r}}(\mathbf{r}')\underbrace{\left[\mathbf{E}^{\text{inc}}_{\zeta,\text{Rx}}\cdot\mathbf{E}^{\text{inc}}_{\zeta,\text{Tx}}\right]_{(\mathbf{r},\omega;\mathbf{r}')}}_{\kappa_{\zeta}^{-1}h^{\text{sc}}_{\zeta}(\mathbf{r},\omega;\mathbf{r}')\ \rightarrow\ \text{kernel}} d\mathbf{r}',\ \mathbf{r}\in S_{\text{a}}$$

scattering occurring at $\mathbf{r}'$

$$S^{\text{sc}}_{\zeta}(\mathbf{r},\omega) = \iiint_{V_{\text{s}}} \Delta\varepsilon_{\text{r}}(\mathbf{r}')\underbrace{h^{\text{sc}}_{\zeta}(\mathbf{r},\omega;\mathbf{r}')}_{\text{data PSF}}d\mathbf{r}'$$

2) solve the linearized problem in Fourier space (*aka* *k*-space, wavenumber space)

- possible if background is assumed uniform → scattering model cast in the form of convolution or cross-correlation in real $(\mathbf{r},\mathbf{r}')$ space

Core Concept: Data Point-spread Function (PSF)

MATHEMATICAL AND PHYSICAL MEANING OF DATA PSF

- object viewed as collection of independent point scatterers
  - response viewed as superposition of scattering from points

$$S_\zeta^{sc}(\mathbf{r},\omega) = \iiint_{V_s} \Delta\varepsilon_r(\mathbf{r}')\, h_\zeta^{sc}(\mathbf{r},\omega;\mathbf{r}')\, d\mathbf{r}'$$

PSF

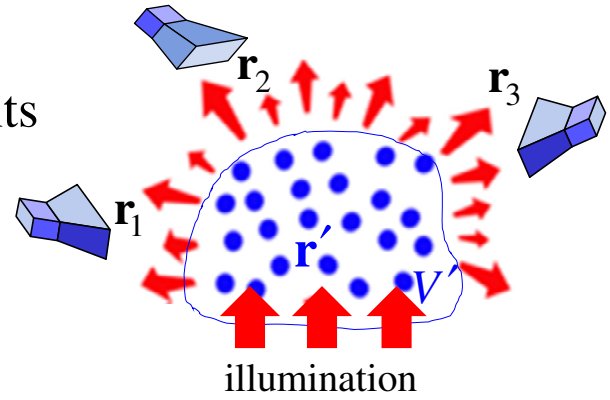

- PSF is the ***system spatial impulse response***
  - response due to point scatterer (3D δ-function)

$$h_\zeta^{sc}(\mathbf{r},\omega;\mathbf{r}_{sp}) = \iiint_{V_s} \delta(\mathbf{r}'-\mathbf{r}_{sp})\, h_\zeta^{sc}(\mathbf{r},\omega;\mathbf{r}')\, d\mathbf{r}'$$

- in homogenous open-boundary background

$$S_\zeta^{sc}(\mathbf{r},\omega) = \underbrace{\iiint_{V_s} \Delta\varepsilon_r(\mathbf{r}')\, h_\zeta^{sc}(\mathbf{r}-\mathbf{r}',\omega)\, d\mathbf{r}'}_{\text{convolution}}$$

  - all we need is $h_\zeta^{sc}(\mathbf{r};\omega), \mathbf{r}' = \mathbf{r}_{sp} = 0$

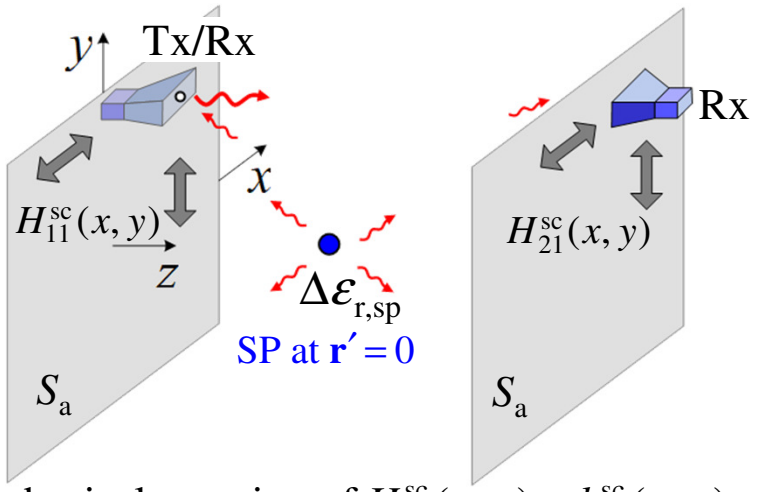

physical meaning of $H_\zeta^{sc}(\mathbf{r};\omega) \sim h_\zeta^{sc}(\mathbf{r};\omega)$

HOW DO WE OBTAIN THE PSF?

$$h_\zeta^{\mathrm{sc}}(\mathbf{r}-\mathbf{r}',\omega) = \kappa_\zeta \mathbf{E}_{\zeta\mathrm{Rx}}^{\mathrm{inc}}(\mathbf{r}'-\mathbf{r},\omega)\cdot\mathbf{E}_{\zeta\mathrm{Tx}}^{\mathrm{inc}}(\mathbf{r}'-\mathbf{r},\omega)$$

1) **analytical expressions** work well for qualitative imaging based on Fresnel-zone and far-field measurements (e.g., SAR)

- example: frequency-domain measurements (VNA, SFCW radar)

Fresnel zone

$$h_\zeta^{\mathrm{sc}}(\mathbf{r}-\mathbf{r}',\omega) \sim \frac{e^{-\mathrm{i}k_\mathrm{b}(\omega)|\mathbf{r}_\mathrm{Tx}-\mathbf{r}'|}}{|\mathbf{r}_\mathrm{Tx}-\mathbf{r}'|}\frac{e^{-\mathrm{i}k_\mathrm{b}(\omega)|\mathbf{r}_\mathrm{Rx}-\mathbf{r}'|}}{|\mathbf{r}_\mathrm{Rx}-\mathbf{r}'|}$$

far zone

$$h_\zeta^{\mathrm{sc}}(\mathbf{r}-\mathbf{r}',\omega) \sim e^{-\mathrm{i}k_\mathrm{b}(\omega)|\mathbf{r}_\mathrm{Tx}-\mathbf{r}'|}\, e^{-\mathrm{i}k_\mathrm{b}(\omega)|\mathbf{r}_\mathrm{Rx}-\mathbf{r}'|}$$

$k_\mathrm{b} = \omega\sqrt{\mu_\mathrm{b}\varepsilon_\mathrm{b}}$

- example: quadrature down-conversion LFM radar at baseband **[Kazemivala *et al.*, *Trans. MTT* 2024]**

complex (I+jQ) signal in time domain

$$h_\zeta^{\mathrm{sc}}(\mathbf{r}-\mathbf{r}',t) \sim \frac{1}{R_\mathrm{Tx}R_\mathrm{Rx}} P\left(\frac{t-\tau_\mathrm{d}}{T_p}\right)\exp\left[-\mathrm{i}2\pi(f_\mathrm{c}\tau_\mathrm{d}+\gamma t\tau_\mathrm{d}-0.5\gamma\tau_\mathrm{d}^2)\right],\ \tau_\mathrm{d}=(R_\mathrm{Tx}+R_\mathrm{Rx})/c$$

$$\tilde{h}_\zeta^{\mathrm{sc}}(\mathbf{r}-\mathbf{r}',f) \sim \underbrace{\mathrm{sinc}\left[T_\mathrm{p}(\gamma\tau_\mathrm{d}+f)\right]}_{\text{mag. peak at } f_\mathrm{m}=-\gamma\tau_\mathrm{d}}\ \underbrace{\exp\left(-\mathrm{i}2\pi f_\mathrm{c}\tau_\mathrm{d}\right)}_{\text{const. in } f\sim\tau_\mathrm{d}}\ \underbrace{\exp\left[-\mathrm{i}2\pi(f+\gamma\tau_\mathrm{d})\tau_\mathrm{d}\right]}_{\substack{\text{zero phase at } f_\mathrm{m}=-\gamma\tau_\mathrm{d} \\ \approx -i2\pi f\tau_\mathrm{d} \text{ (linear in } f\text{)}}}\ \underbrace{\exp\left(\mathrm{i}\pi\gamma\tau_\mathrm{d}^2\right)}_{\approx 1\text{, can ignore}}$$

complex (I+jQ) signal in frequency domain

HOW DO WE OBTAIN THE PSF? cont.

2) simulated antenna incident-field distributions [Amineh *et al.*, *Int. J. Biomed. Imaging* 2012, *IEEE Trans. IM* 2015]

$$h_\zeta^{\mathrm{sc}}(\mathbf{r},\omega)\Big|_{\mathbf{r}'=0} = \kappa_\zeta \mathbf{E}^{\mathrm{inc}}_{\zeta\mathrm{Rx}}(-\mathbf{r},\omega)\cdot\mathbf{E}^{\mathrm{inc}}_{\zeta\mathrm{Tx}}(-\mathbf{r},\omega)\Big|_{\mathbf{r}'=0}$$

$\mathbf{r}'=0$ (origin at scattering point) ⟷ *reciprocity*

antenna pair position during scan

$$= \kappa_\zeta \mathbf{E}^{\mathrm{inc}}_{\zeta\mathrm{Rx}}(\mathbf{r}',\omega)\cdot\mathbf{E}^{\mathrm{inc}}_{\zeta\mathrm{Tx}}(\mathbf{r}',\omega)\Big|_{\mathbf{r}=0}$$

$\mathbf{r}=0$ (origin at antenna)

3) simulated PSFs with scattering probe (SP) at origin

4) measured PSFs with SP at origin
enables extreme near-field imaging and quantitative imaging

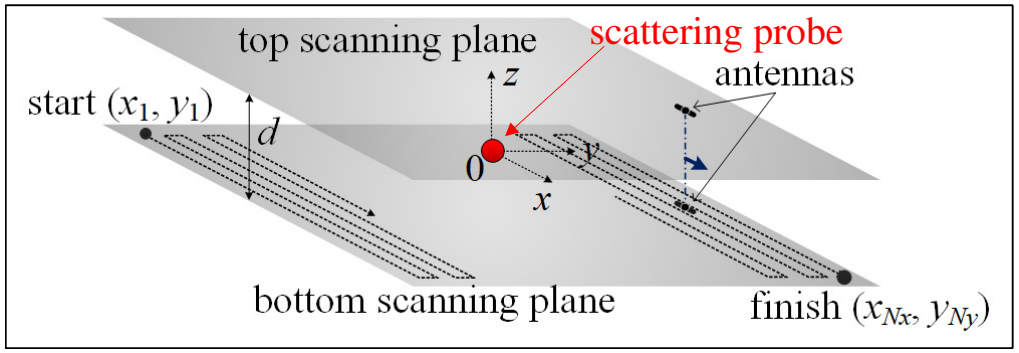

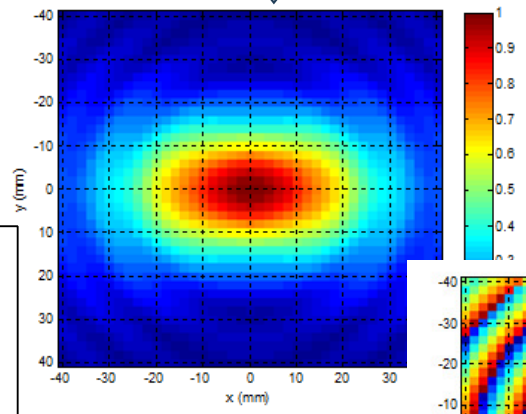

PSF magnitude

PSF phase

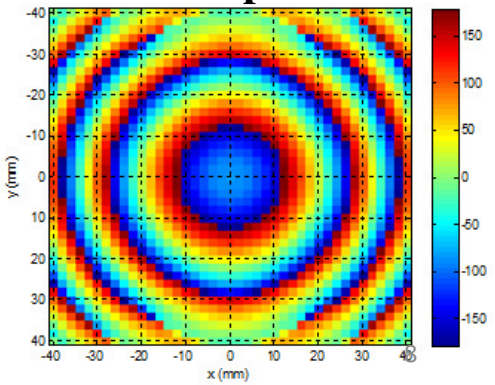

[Amineh *et al.*, *IEEE Trans. Instrum. Meas.*, 2015]

MEASURED PSF WITH KNOWN SCATTERING PROBE (SP)

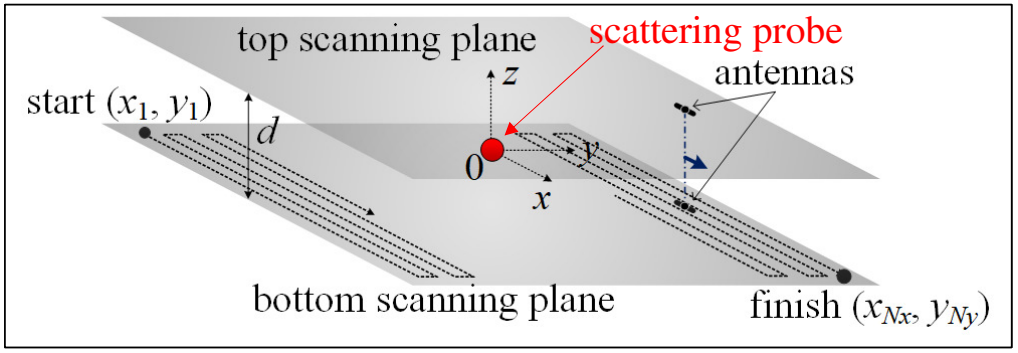

scattering probe (SP) parameters

- volume Ω_{sp}
- relative permittivity $\varepsilon_{r,sp}$

- SP contrast *vs.* ideal $\delta(\mathbf{r}')$ scatterer (matters in quantitative imaging)

$$\iiint_{V'} \delta(\mathbf{r}')d\mathbf{r}' = 1 \leftrightarrow \iiint_{\Omega_{sp}} \Delta\varepsilon_{r,sp}d\mathbf{r}' = \Delta\varepsilon_{r,sp}\Omega_{sp}$$

- measured response with SP as point scatterer: $H_\zeta^{sc}(\mathbf{r},\omega)$

$$\Rightarrow H_\zeta^{sc}(\mathbf{r},\omega)\Big|_{\mathbf{r}'=0} = \Delta\varepsilon_{r,sp}\Omega_{sp}\, h_\zeta^{sc}(\mathbf{r},\omega)\Big|_{\mathbf{r}'=0} \Rightarrow h_\zeta^{sc}(\mathbf{r},\omega)\Big|_{\mathbf{r}'=0} = \frac{H_\zeta^{sc}(\mathbf{r},\omega)\Big|_{\mathbf{r}'=0}}{\Delta\varepsilon_r\Omega_{sp}}$$

- data equation in terms of $H_\zeta^{sc}(\mathbf{r},\omega)$:

$$S_\zeta^{sc}(\mathbf{r},\omega) = \frac{1}{\Delta\varepsilon_{r,sp}\Omega_{sp}} \iiint_{V_s} \Delta\varepsilon_r(\mathbf{r}')\, H_\zeta^{sc}(\mathbf{r}-\mathbf{r}',\omega)d\mathbf{r}'$$

EXAMPLE: SIMULATED-FIELD *vs*. MEASURED-PSF MODEL

[Amineh *et al.*, *IEEE Trans. Instrum. Meas.*, 2015]

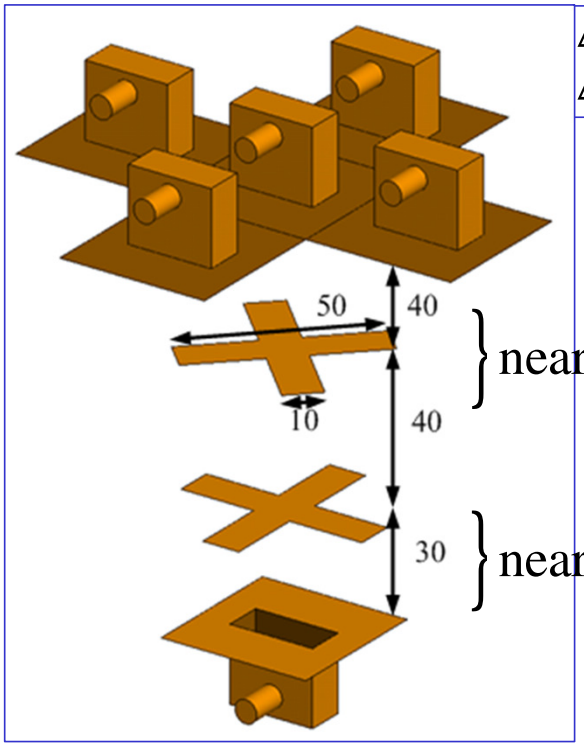

$\Delta x = \Delta y = 5\,\text{mm}$
$\Delta f = 250\,\text{MHz}$

X-band (WR90) open-end waveguides ($f_c \approx 6.56\,\text{GHz}$)

f (GHz)	λ (mm)	D_{far} (mm)
$3 < f_c$	100	12.5
8.2	37	34
20	15	83

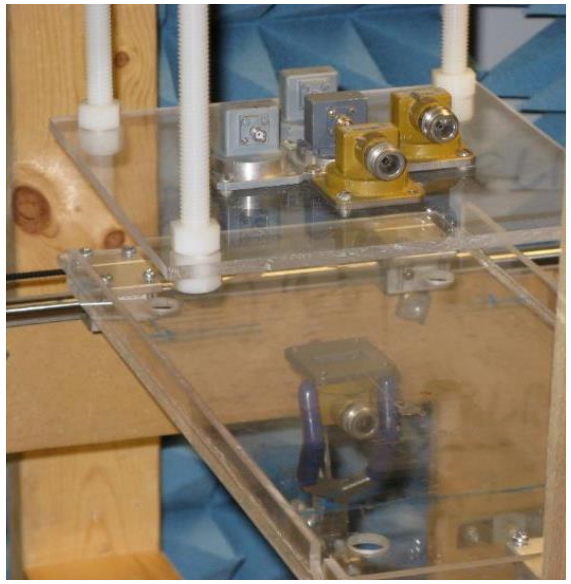

[photo credit: Justin McCombe]

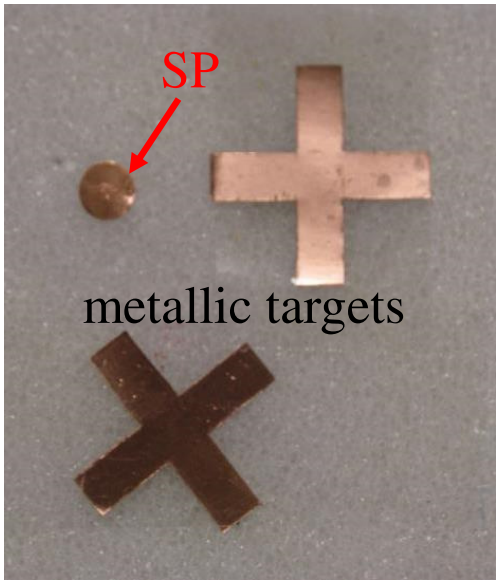

METALLIC-TARGET IMAGES WITH PSF FROM SIMULATED INCIDENT FIELDS

microwave-holography (MH) images

[Amineh *et al.*, *Trans. Instrum. Meas.*, 2015]

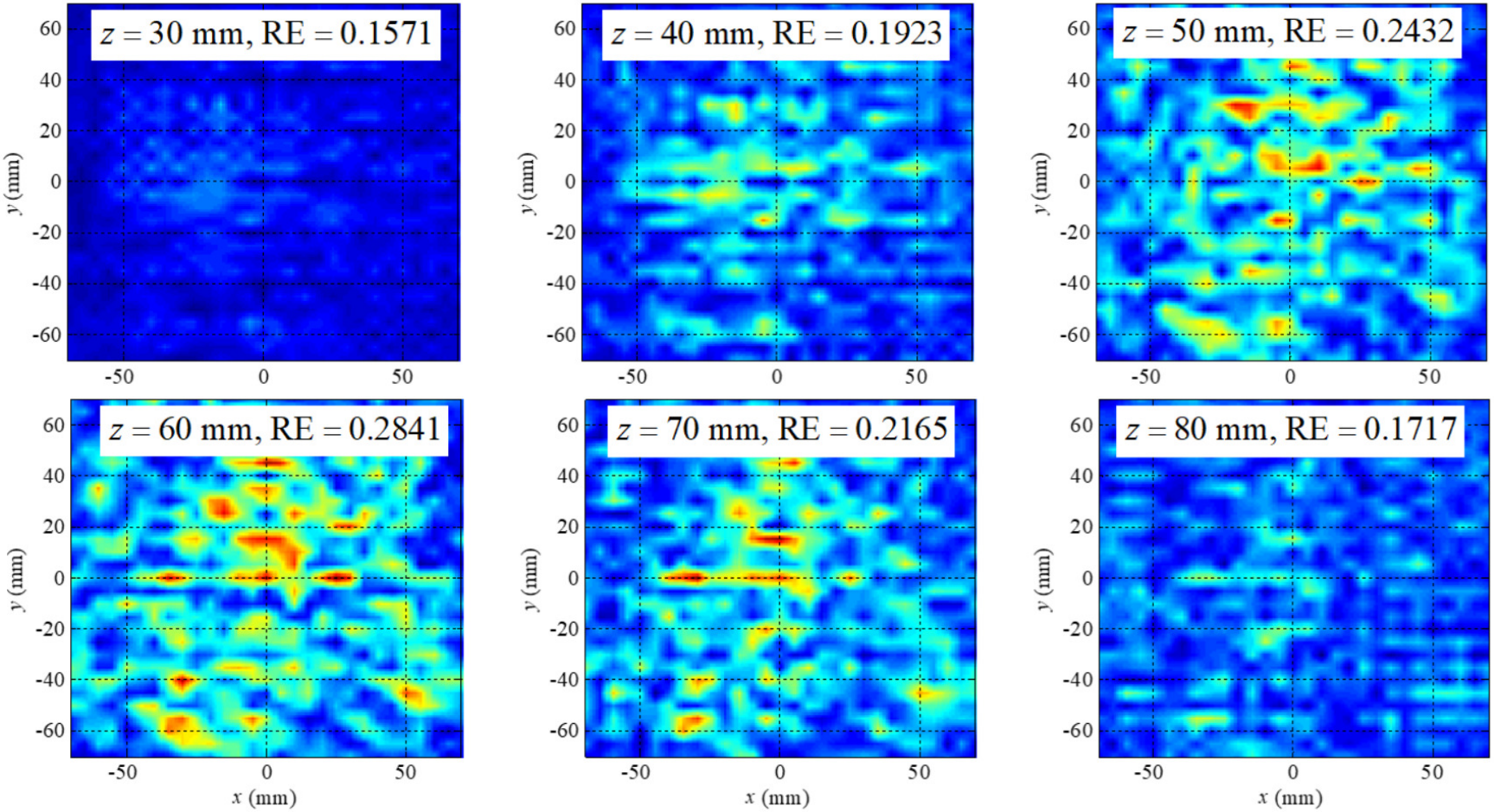

METALLIC-TARGET MH IMAGES WITH PSF FROM MEASUREMENTS

microwave-holography (MH) images

[Amineh *et al.*, *Trans. Instrum. Meas.*, 2015]

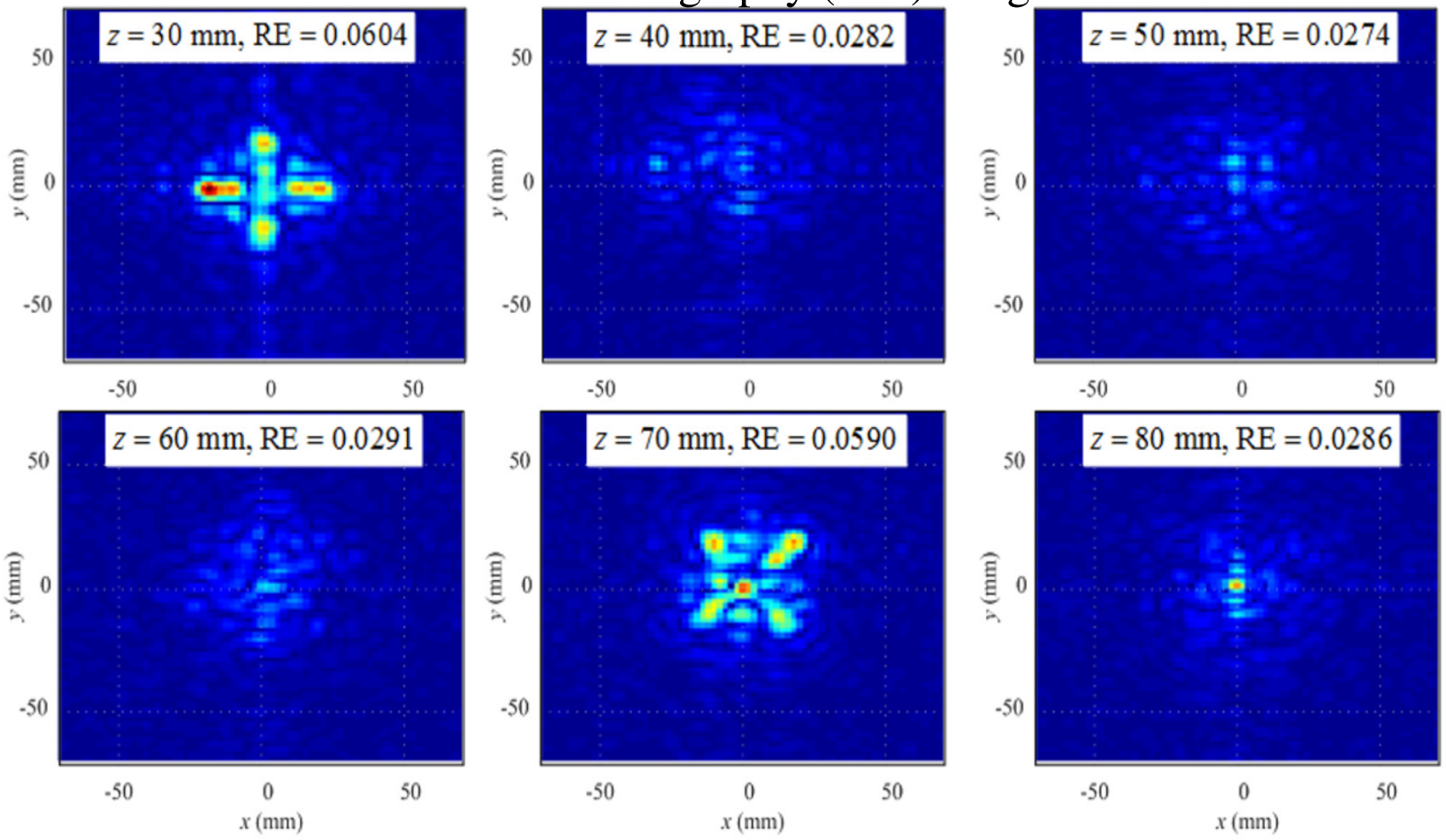

EXAMPLE: MEASUREMENT PROVIDING PSF IN BREAST-PHANTOM IMAGING

[photo credit: Daniel Tajik]

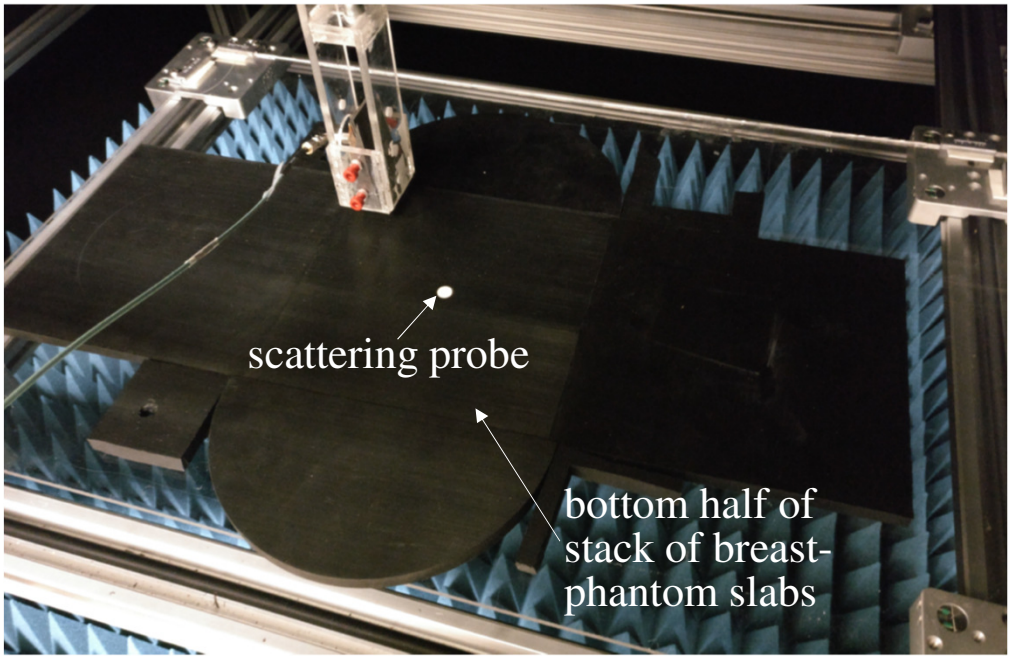

measured PSF

$$H_{\zeta}^{\mathrm{sc}}(\mathbf{r},\omega)$$

$$\left|H_{12}^{\mathrm{sc}}(x,y,f=5.5\,\mathrm{GHz})\right|$$

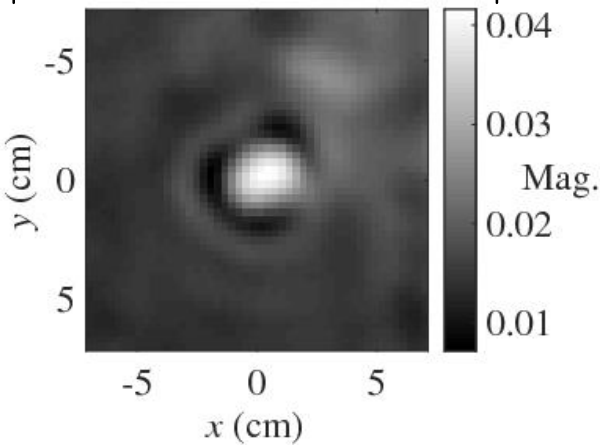

calibration object with small scattering probe at center

$\varepsilon_{\mathrm{r,sp}} \approx 18 - \mathrm{i}0.05$, radius 5 mm, height 10 mm

[Tajik *et al.*, *IEEE J-ERM*, 2020]

COMPARISON OF ANALYTICAL, SIMULATED & MEASURED PSFs

Type of PSF	Account for Antennas'			Other Sources of Model Inaccuracies
	near-field	pattern	mutual coupling	
Analytical PSF	no	no	no	background clutter
Simulated Incident Fields	yes	yes	depends	background clutter numerical modeling errors
Simulated PSF with SP	yes	yes	depends	background clutter numerical modeling errors
Measured PSF with SP	yes	yes	yes	insufficient SNR if SP is too far

- measured PSFs provide the ***best model accuracy*** and allow for ***quantitative image reconstruction***
- BUT there are limitations
  - SP must be small ($< \lambda_{min}/4$)
  - small SP leads to poor SNR with far-zone measurements

Image Reconstruction with Quantitative Microwave Holography (QMH)

(direct solution of the data equation in Fourier space)

QMH WITH PLANAR SCANNING

- in real space (planar scanning)

2D convolution in (x,y)

$$\underbrace{S_\zeta^{\mathrm{sc}}(x,y,\overline{z},\omega)}_{\text{data}} \approx \frac{1}{\Delta\varepsilon_{\mathrm{r,sp}}\Omega_{\mathrm{sp}}} \int_{x'}\int_{y'}\int_{z'} \underbrace{\Delta\varepsilon_{\mathrm{r}}(x',y',z')}_{\text{unknown permittivity}} \underbrace{H_\zeta^{\mathrm{sc}}(x-x',y-y',\overline{z},\omega;z')}_{\text{PSF}} dx'dy'dz', \quad \zeta = 1,\ldots,N_{\mathrm{T}}$$

- in *Fourier-range* (or kz) space ⇩ 2D FFT $(x,y) \leftrightarrow (k_x,k_y)$

$$\tilde{S}_\zeta(k_x,k_y,\overline{z},\omega) \approx \frac{\Delta x'\Delta y'}{\Delta\varepsilon_{\mathrm{r,sp}}\Omega_{\mathrm{sp}}} \int_{z'} \Delta\tilde{\varepsilon}_{\mathrm{r}}(k_x,k_y,z')\,\tilde{H}_\zeta(k_x,k_y,\overline{z},\omega;z')\,dz'$$

- discretize integral along z' into a sum
- solve system of equations ***at each spectral position***: $\boldsymbol{\kappa} \equiv (k_x,k_y)$

$$\tilde{S}_\zeta(\boldsymbol{\kappa},\omega_k) \approx \sum_{q=1}^{N_z} \tilde{\rho}(\boldsymbol{\kappa},z_q')\left[\tilde{H}_\zeta(\boldsymbol{\kappa},\omega_k,z_q')\right], \quad \begin{matrix} k=1,\ldots,N_\omega \\ \zeta=1,\ldots,N_{\mathrm{T}} \end{matrix}$$

$$\tilde{\rho}(\boldsymbol{\kappa},z_q') = \frac{\Delta x'\Delta y'\Delta z'}{\Delta\varepsilon_{\mathrm{r,sp}}\Omega_{\mathrm{sp}}} \Delta\tilde{\varepsilon}_{\mathrm{r}}(\boldsymbol{\kappa},z_q') \qquad \Omega_{\mathrm{v}} = \Delta x'\Delta y'\Delta z'$$

- recover contrast in real space with 2D IFFT: $\Delta\varepsilon_{\mathrm{r}}(x',y',z_q') = \mathrm{IFFT}_{2\mathrm{D}}\left\{\Delta\tilde{\varepsilon}_{\mathrm{r}}(k_x,k_y,z_q')\right\}$, $q=1,\ldots,N_z$

QMH SYSTEMS OF EQUATIONS SOLVED IN *kz* SPACE: MATRIX COMPOSITION

system of equations solved at each k-space point $\boldsymbol{\kappa}_{ij}$

$$\tilde{S}_\zeta(\boldsymbol{\kappa}_{ij},\omega_k) \approx \sum_{q=1}^{N_z} \tilde{\rho}(\boldsymbol{\kappa}_{ij},z_q')\tilde{H}_\zeta(\boldsymbol{\kappa}_{ij},\omega_k,z_q')$$

$k=1,\ldots,N_\omega$, $\zeta=1,\ldots,N_\mathrm{T}$ ⇨ $N_\omega N_\mathrm{T}$ equations for N_z unknowns

⇨ $$\mathbf{H}(\boldsymbol{\kappa}_{ij})_{[N_\mathrm{T}N_\omega\times N_z]}\,\boldsymbol{\rho}(\boldsymbol{\kappa}_{ij})_{[N_z\times 1]} = \mathbf{d}(\boldsymbol{\kappa}_{ij})_{[N_\mathrm{T}N_\omega\times 1]}$$

$\boldsymbol{\kappa}_{ij} = (i\Delta k_x, j\Delta k_y)$
$i=1,\ldots,N_x;\ j=1,\ldots,N_y$

vector of unknowns: $\boldsymbol{\rho}(\boldsymbol{\kappa}_{ij}) = \left[\tilde{\rho}(\boldsymbol{\kappa}_{ij},z_1') \ \cdots \ \tilde{\rho}(\boldsymbol{\kappa}_{ij},z_{N_z}')\right]^T_{N_z\times 1}$

***data vector*:**

$$\mathbf{d}(\boldsymbol{\kappa}_{ij}) = \begin{bmatrix} \underline{\mathbf{d}}(\boldsymbol{\kappa}_{ij},\omega_1) \\ \vdots \\ \underline{\mathbf{d}}(\boldsymbol{\kappa}_{ij},\omega_{N_\omega}) \end{bmatrix}_{N_\omega N_\mathrm{T}\times 1}, \text{ where}$$

$$\underline{\mathbf{d}}(\boldsymbol{\kappa}_{ij},\omega_k) = \begin{bmatrix} \tilde{S}_1(\boldsymbol{\kappa}_{ij},\omega_k) \\ \vdots \\ \tilde{S}_{N_\mathrm{T}}(\boldsymbol{\kappa}_{ij},\omega_k \end{bmatrix}_{N_\mathrm{T}\times 1}, \ k=1,\ldots,N_\omega$$

***system matrix*:**

$$\mathbf{H}(\boldsymbol{\kappa}_{ij}) = \begin{bmatrix} \underline{\mathbf{H}}(\boldsymbol{\kappa}_{ij},\omega_1,z_1') & \cdots & \underline{\mathbf{H}}(\boldsymbol{\kappa}_{ij},\omega_1,z_{N_z}') \\ \vdots & \ddots & \vdots \\ \underline{\mathbf{H}}(\boldsymbol{\kappa}_{ij},\omega_{N_\omega},z_1') & \cdots & \underline{\mathbf{H}}(\boldsymbol{\kappa}_{ij},\omega_{N_\omega},z_{N_z}') \end{bmatrix}_{N_\mathrm{T}N_\omega\times N_z}, \text{ where}$$

$$\underline{\mathbf{H}}(\boldsymbol{\kappa}_{ij},\omega_k,z_q') = \begin{bmatrix} \tilde{H}_1(\boldsymbol{\kappa}_{ij},\omega_k,z_q') \\ \vdots \\ \tilde{H}_{N_\mathrm{T}}(\boldsymbol{\kappa}_{ij},\omega_k,z_q') \end{bmatrix}_{N_\mathrm{T}\times 1}, \ \begin{matrix} k=1,\ldots,N_\omega \\ q=1,\ldots,N_z \end{matrix}$$

COMPUTATIONAL ADVANTAGES OF SOLVING IN *kz* SPACE

$$\mathbf{H}(\boldsymbol{\kappa}_{ij})_{[N_T N_\omega \times N_z]}\,\boldsymbol{\rho}(\boldsymbol{\kappa}_{ij})_{[N_z \times 1]} = \mathbf{d}(\boldsymbol{\kappa}_{ij})_{[N_T N_\omega \times 1]}$$

$$\boldsymbol{\kappa}_{ij} = (i\Delta k_x,\, j\Delta k_y)$$
$$i = 1,\ldots,N_x;\;\; j = 1,\ldots,N_y$$

- we solve $N_S = N_x N_y$ systems ($N_S \sim 10^4$ samples on synthetic aperture)
- size of each system is small: $N_T N_\omega \times N_z$ (e.g. 60×5)
- typical execution times for all N_S systems: ~1 s on laptop with *Matlab* $\rightarrow O(N_x N_y N_z^3)$
- solution is several orders of magnitude faster than solving in real space, where system matrix size is: $N_D \times N_v$ with $N_D = N_x N_y N_z N_T N_\omega \sim 10^6$ to 10^8, $N_v = N_x N_y N_z \sim 10^5$ to 10^6 $\rightarrow O(N_x^3 N_y^3 N_z^3)$

SUMMARY: QUANTITATIVE MICROWAVE HOLOGRAPHY (QMH)

input

data & PSFs on uniform grid: $S_\zeta^{\mathrm{sc}}(x, y, \overline{z}, \omega)$, $H_\zeta^{\mathrm{sc}}(x, y, \overline{z}, \omega; 0, 0, z')$

$$\tilde{H}_\zeta^{\mathrm{sc}}(\boldsymbol{\kappa}, \omega; z') = \mathrm{FT}_{2\mathrm{D}}\left\{H_\zeta^{\mathrm{sc}}(x, y, \overline{z}, \omega; z')\right\}$$

$$\tilde{S}_\zeta^{\mathrm{sc}}(\boldsymbol{\kappa}, \omega) = \mathrm{FT}_{2\mathrm{D}}\left\{S_\zeta^{\mathrm{sc}}(x, y, \overline{z}, \omega)\right\}$$

$$\mathbf{H}(\boldsymbol{\kappa}_{ij})_{[N_{\mathrm{T}}N_\omega \times N_z]}\, \boldsymbol{\rho}(\boldsymbol{\kappa}_{ij})_{[N_z \times 1]} = \mathbf{d}(\boldsymbol{\kappa}_{ij})_{[N_{\mathrm{T}}N_\omega \times 1]}$$

$$\Delta\varepsilon_{\mathrm{r}}(x', y', z') = \Delta\varepsilon_{\mathrm{r,sp}}\Omega_{\mathrm{sp}}\Omega_{\mathrm{v}}^{-1}\mathrm{FT}_{2\mathrm{D}}^{-1}\left\{\tilde{\rho}(\boldsymbol{\kappa}; z')\right\}$$

output

EXAMPLE: 2D IMAGING OF COMPRESSED BREAST PHANTOM – SFCW DATA

- compressed-breast phantom (18×19×5.5 cm^3) with tumor simulants at 2 range positions
- mechanical scan, 20×20 cm^2 ($\Delta_{x,y}$ =3 mm), 3 GHz - 8 GHz SFCW (Δ_f =100 MHz), S_{21}

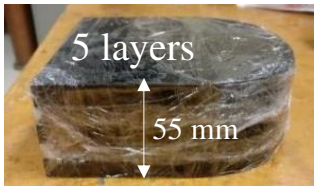

[Tajik *et al.*, *IEEE Trans. MTT* 2022]

CT IMAGE SLICES

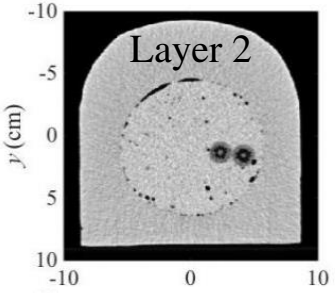

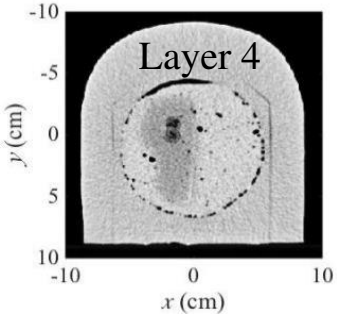

PHANTOM AVERAGED DIELECTRIC PROPERTIES (3 GHZ TO 8 GHZ)

Material (Structure)	ϵ'	ϵ''
Carbon-rubber Sheet (Averaged Breast Tissue)	10.91	2.84
Embedding/Matching Medium	10.41	5.07
Tumour Simulant	55.27	16.63
Fibroglandular Tissue Simulant	23.83	11.27
Scattering Probe (PSF)	50.00	0.05

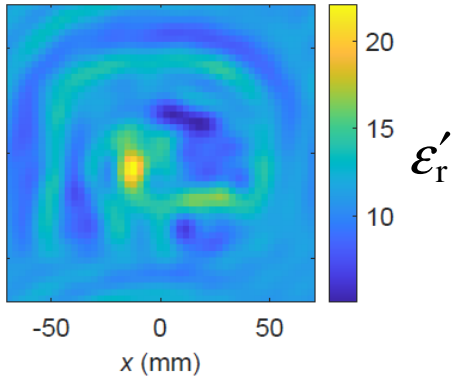

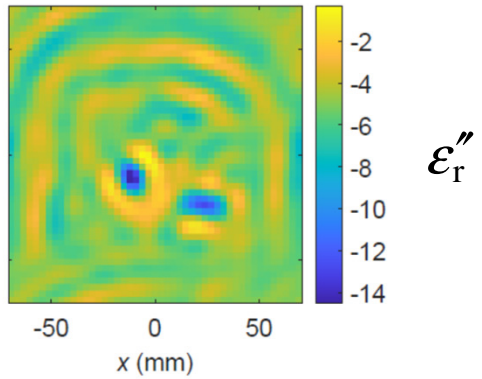

2D projection QMH quantitative images

EXAMPLE: 3D mm-WAVE IMAGING WITH SFCW DATA

- four *Styrofoam* sheets (30×30×5.1 cm^3) with various objects at 4 range positions
- mechanical scan, 20×20 cm^2 ($\Delta_{x,y}$ =2 mm), 26-40 GHz SFCW (Δ_f =100 MHz), S_{11}

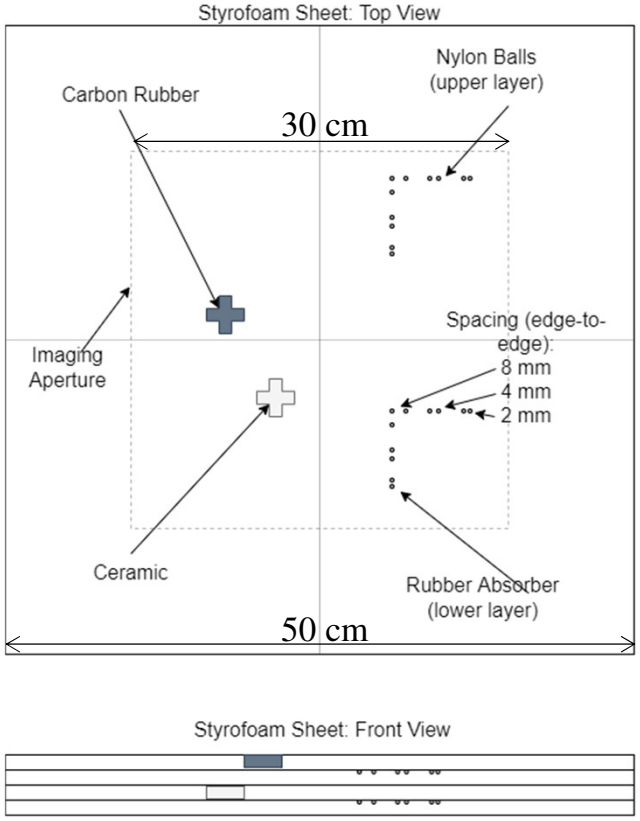

[Tajik *et al.*, *IEEE Trans. MTT* 2022]

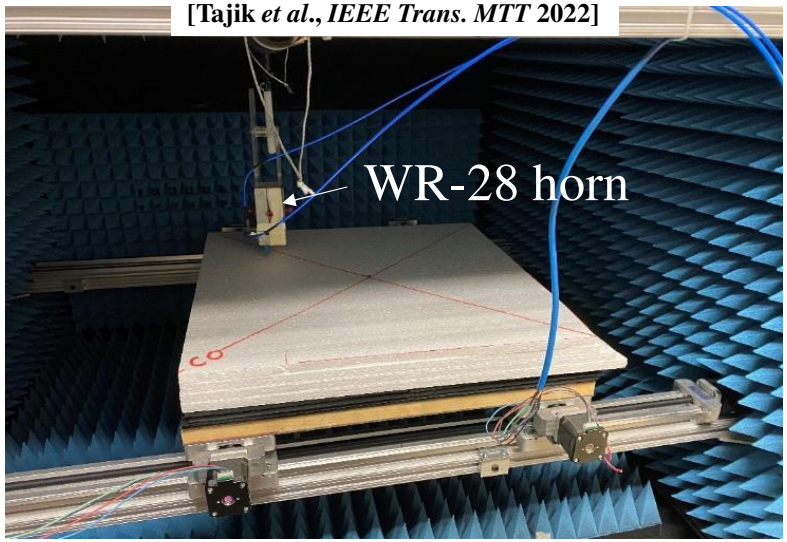

Material (Structure)	ϵ'	ϵ''
Styrofoam	1.18	0.00
Nylon Ball [38]	3.05	0.03
Carbon Rubber Cross*	8.49	0.93
Ceramic Cross*	4.48	0.44
Carbon Rubber Scattering Probe*	7.85	3.01

EXAMPLE: 3D mm-WAVE IMAGING WITH SFCW (VNA) DATA, cont.

[Tajik *et al.*, *IEEE Trans. MTT* 2022]

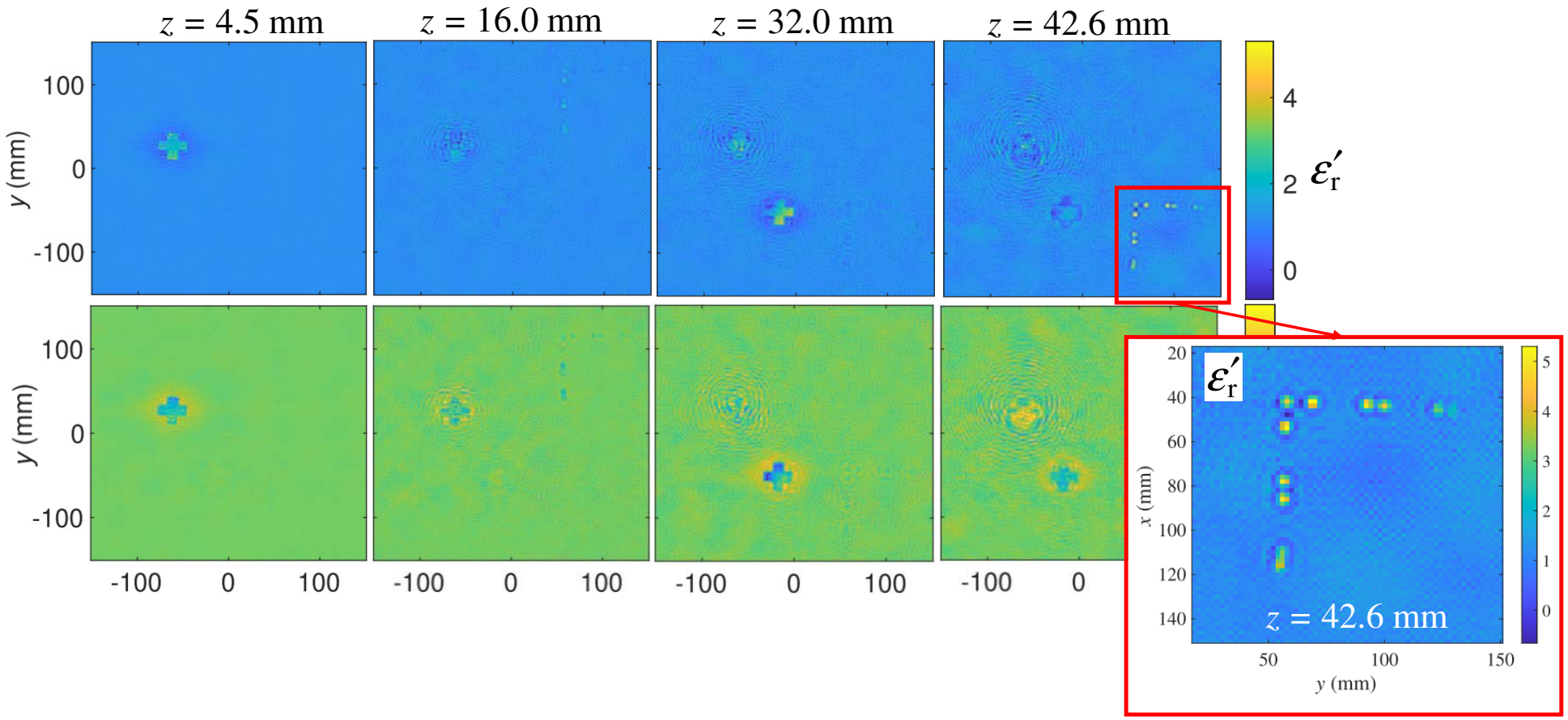

Image Reconstruction with Scattered Power Mapping (SPM)

(projection-based image reconstruction followed by image deconvolution)

SPM MATHEMATICAL BASIS

[Tu *et al.*, *Inv. Problems* 2015] [Shumakov *et al.*, *IEEE Trans. MTT* 2018][Nikolova, *Introduction to Microwave Imaging*, 2017]

SPM Stage 1 (projection-based image reconstruction)

imaged position *measurement position* *imaged position*

$$\underbrace{M(\mathbf{r}')}_{\text{OUT scattered power map}} = \sum_{\zeta=1}^{N_T} \int_\omega \iint_{\mathbf{r}\in S_a} \underbrace{S_\zeta^{sc}(\mathbf{r},\omega)}_{\text{OUT data}} \left[\underbrace{H_\zeta^{sc}(\mathbf{r}-\mathbf{r}';\omega)}_{\text{PSF}} \right]^* d\mathbf{r}\, d\omega$$

data equation $$S_\zeta^{sc}(\mathbf{r},\omega) = \frac{1}{\Delta\varepsilon_{r,sp}\Omega_{sp}} \iiint_{V_s} \Delta\varepsilon_r(\mathbf{r}')\, H_\zeta^{sc}(\mathbf{r}-\mathbf{r}',\omega)\, d\mathbf{r}'$$

SPM Stage 2 (image deconvolution)

$$M(\mathbf{r}') = \frac{1}{\Delta\varepsilon_{r,sp}\Omega_{sp}} \iiint_{V_s} \Delta\varepsilon_r(\mathbf{r}'')\, \underbrace{M^H_{sp@\mathbf{r}'}(\mathbf{r}')}_{\text{SP scattered power map}} d\mathbf{r}''$$

$$M^H_{sp@\mathbf{r}'}(\mathbf{r}') = \sum_{\zeta=1}^{N_T} \int_\omega \iint_{S_a} \underbrace{H_\zeta^{sc}(\mathbf{r}-\mathbf{r}'',\omega)}_{\text{data for SP@}\mathbf{r}''} \left[\underbrace{H_\zeta^{sc}(\mathbf{r}-\mathbf{r}',\omega)}_{\text{PSF}} \right]^* d\mathbf{r}\, d\omega$$

SPM IMAGE RECONSTRUCTION STAGE 1 (real space)

SPM Stage 1 image formation:

$$M(\mathbf{r}') = \sum_{\zeta=1}^{N_\mathrm{T}} \int_\omega \iint_{\mathbf{r}\in S_\mathrm{a}} S_\zeta^{\mathrm{sc}}(\mathbf{r},\omega)\left[H_\zeta^{\mathrm{sc}}(\mathbf{r}-\mathbf{r}';\omega)\right]^* d\mathbf{r}\, d\omega$$

imaged position — $M(\mathbf{r}')$; *measurement position* — $S_\zeta^{\mathrm{sc}}(\mathbf{r},\omega)$; *imaged position* — $H_\zeta^{\mathrm{sc}}(\mathbf{r}-\mathbf{r}';\omega)$

- mathematical insight: ***scattered-power map*** $M(\mathbf{r}')$ is the ***projection*** of data (S_ζ^{sc}) onto the PSF (H_ζ^{sc}) functional space (inner product in the data space $(\mathbf{r},\omega,\zeta)$)
  - ➢ thus, $M(\mathbf{r}')$ plots the ***aggregate complex-valued similarity*** at $\mathbf{r}'$ between the OUT responses and the respective PSF responses due to a point scatterer at $\mathbf{r}'$

- SPM works with time-domain signals as well

[R. Kazemivala *et al.*, *IEEE Trans. MTT*, 2024]

$$M(\mathbf{r}') = \sum_{\zeta=1}^{N_\mathrm{T}} \int_\omega \iint_{\mathbf{r}\in S_\mathrm{a}} \mathcal{F}_t\underbrace{\left\{S_\zeta^{\mathrm{sc}}(\mathbf{r},t)\otimes H_\zeta^{\mathrm{sc}}(\mathbf{r}-\mathbf{r}';t)\right\}}_{\text{cross-correlation } X_\zeta(\tau),\tau(\mathbf{r}-\mathbf{r}')} d\mathbf{r}\, d\omega = \sum_{\zeta=1}^{N_\mathrm{T}} \int_t \iint_{\mathbf{r}\in S_\mathrm{a}} S_\zeta^{\mathrm{sc}}(\mathbf{r},t)\left[H_\zeta^{\mathrm{sc}}(\mathbf{r}-\mathbf{r}';t)\right]^* d\mathbf{r}\, dt$$

assuming infinite bandwidth $\omega\in[0,\infty)$

IMPLEMENTATION OF SPM STAGE 1 (real space)

- replace integrals with sums

measurement position *imaged position*

Stage 1 image: $$M(\mathbf{r}'_q) = \sum_{\zeta=1}^{N_T} \sum_{k=1}^{N_\omega} \sum_{p=1}^{N_S} S_\zeta^{sc}(\mathbf{r}_p, \omega_k) \left[H_\zeta^{sc}(\mathbf{r}_p - \mathbf{r}'_q; \omega_k) \right]^*, \quad q = 1, \ldots, N_v$$

- reconstruction involves only products and sums – **no systems of equations solved**!
- ill-posedness is *not* a concern: systems of equations are not solved
- reconstruction can be carried out with ANY set of measurement points $\mathbf{r}_p$, $p = 1, \ldots, N_S$, (uniform grid on aperture, random sampling in 2D or 3D)
- scattered power map $M(\mathbf{r}'_q)$, $q = 1, \ldots, N_v$, is on uniform grid (2D or 3D)
- image $|M(\mathbf{r}')|$ is only qualitative, usually normalized, $|M(\mathbf{r}')| / |M(\mathbf{r}')|_{max}$
- data abundance (large N_S, N_ω, N_T) is critical: (i) reduces image artifacts due to measurement noise and clutter, and (ii) improves image spatial resolution

SPM STAGE 1 IMAGE RECONSTRUCTION (Fourier space)

- with sampling on uniform grid, SPM Stage 1 is accelerated with 2D FFT

$$H_\zeta^{\mathrm{sc}}(x,y,\bar{z},\omega;x',y',z') \equiv H_\zeta^{\mathrm{sc}}\left(x-x',y-y',\bar{z};\omega;z'\right)$$

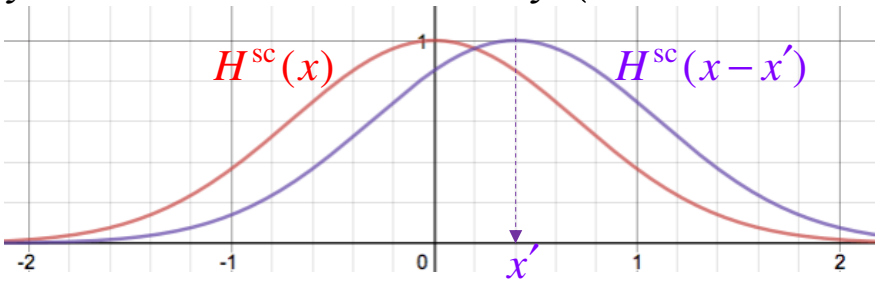

⇦ *PSF shifts to the right when probe shifts to the right, $x' > 0$*

planar data

$$M(x',y',z') = \sum_{\zeta=1}^{N_{\mathrm{T}}}\sum_{k=1}^{N_\omega} \underbrace{\iint_{S_a} S_\zeta^{\mathrm{sc}}(x,y,\bar{z},\omega_k)\left[H_\zeta^{\mathrm{sc}}\left(x-x',y-y',\bar{z},\omega_k;z'\right)\right]^* dxdy}_{\text{cross-correlation in } x \text{ and } y:\ S_\zeta^{\mathrm{sc}}(x,y,\bar{z},\omega_k)\otimes H_\zeta^{\mathrm{sc}}(x,y,\bar{z},\omega_k;z')}$$

- take 2D FT of both sides → OUT power map in 2D Fourier space (kz-space)

$$\tilde{M}(\underbrace{k_x,k_y}_{\kappa},z') = \sum_{\zeta=1}^{N_{\mathrm{T}}}\sum_{k=1}^{N_\omega} \underbrace{\tilde{S}_\zeta^{\mathrm{sc}}(k_x,k_y,\bar{z},\omega_k)}_{\text{2D FT of data}}\left[\underbrace{\tilde{H}_\zeta\left(k_x,k_y,\bar{z},\omega_k;z'\right)}_{\text{2D FT of projection basis}}\right]^*$$

$$\Rightarrow M(x',y',z') = \mathrm{IFFT}_{2\mathrm{D}}\left\{\tilde{M}(k_x,k_y,z')\right\}$$

REAL *vs.* FOURIER SPACE IMPLEMENTATIONS OF SPM STAGE 1

real space: $$M(\mathbf{r}_q') = \sum_{\zeta=1}^{N_\mathrm{T}} \sum_{k=1}^{N_\omega} \sum_{p=1}^{N_\mathrm{S}} S_\zeta^{\mathrm{sc}}(\mathbf{r}_p, \omega_k) \left[H_\zeta^{\mathrm{sc}}(\mathbf{r}_p - \mathbf{r}_q'; \omega_k) \right]^*, \quad q = 1, \ldots, N_\mathrm{v}$$

kz space: $$\tilde{M}(\boldsymbol{\kappa}_{ij}, z_q') = \sum_{\zeta=1}^{N_\mathrm{T}} \sum_{k=1}^{N_\omega} \tilde{S}_\zeta^{\mathrm{sc}}(\boldsymbol{\kappa}_{ij}, \overline{z}, \omega_k) \left[\tilde{H}_\zeta\left(\boldsymbol{\kappa}_{ij}, \overline{z}, \omega_k; z_q'\right) \right]^*$$

$$\begin{aligned} &q = 1, \ldots, N_z \\ &\boldsymbol{\kappa}_{ij} = (i\Delta k_x, j\Delta k_y) \\ &\left.\begin{aligned} i &= 1, \ldots, N_x \\ j &= 1, \ldots, N_y \end{aligned}\right\} N_\mathrm{S} = N_x N_y \end{aligned}$$

SPM Stage 1 in real space

- slower

  FLOPs ~ $N_\mathrm{v} N_\mathrm{S} N_\omega N_\mathrm{T} \approx N_\mathrm{v}^2 N_\omega N_\mathrm{T}$
- BUT can run in parallel with measurements
- can process randomly sampled data in 3D space (image still on uniform grid)
- suited for imaging with random sampling

SPM Stage 1 in Fourier (*kz*) space

- faster

  FLOPs ~ $N_\mathrm{S} N_z N_\omega N_\mathrm{T} \approx N_\mathrm{v} N_\omega N_\mathrm{T}$
- needs uniform sampling on canonical aperture (planar, cylindrical) to employ 2D FFT
- needs measurement to be completed before starting reconstruction

SIMULATION EXAMPLE: SPM STAGE 1 IMAGE OF F-SHAPE

simulation of PSF acquisition

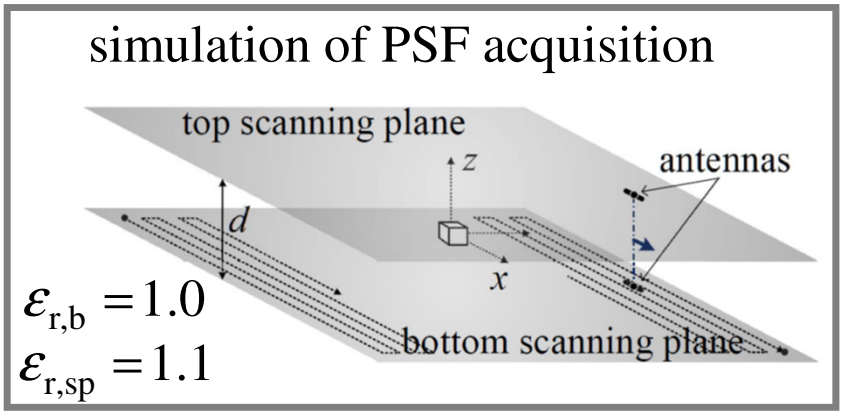

simulation of data acquisition

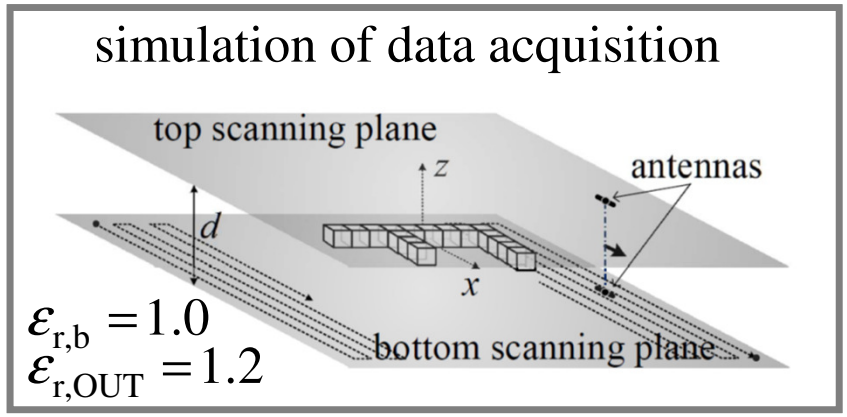

Altair FEKO

- aperture span 20×20 cm^2, d = 5 cm
- $\Delta_{x,y}$ = 1 cm (λ_{min} /2 = 9.4 mm)
- frequency span 3-16 GHz
- Δ_f = 1 GHz

sample PSF: S_{11} at 4 GHz MAG/PHASE

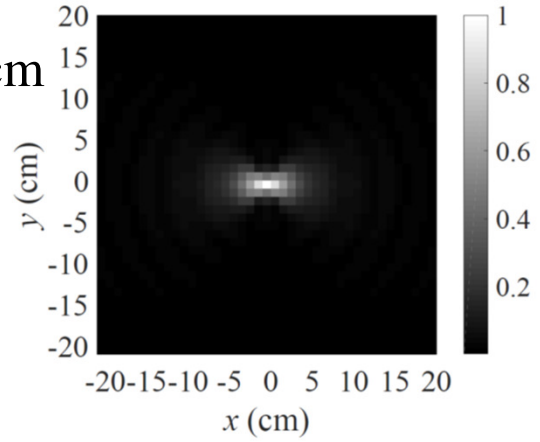

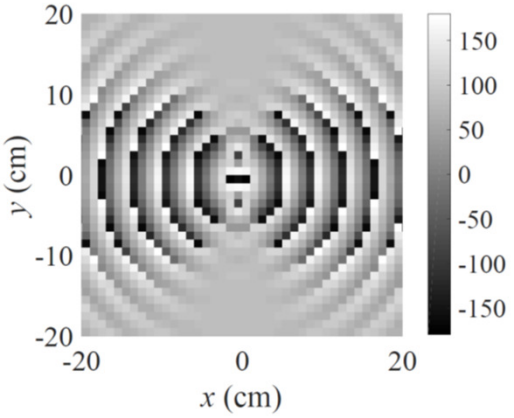

SIMULATION EXAMPLE: SPM STAGE 1 IMAGE OF F-SHAPE, cont.

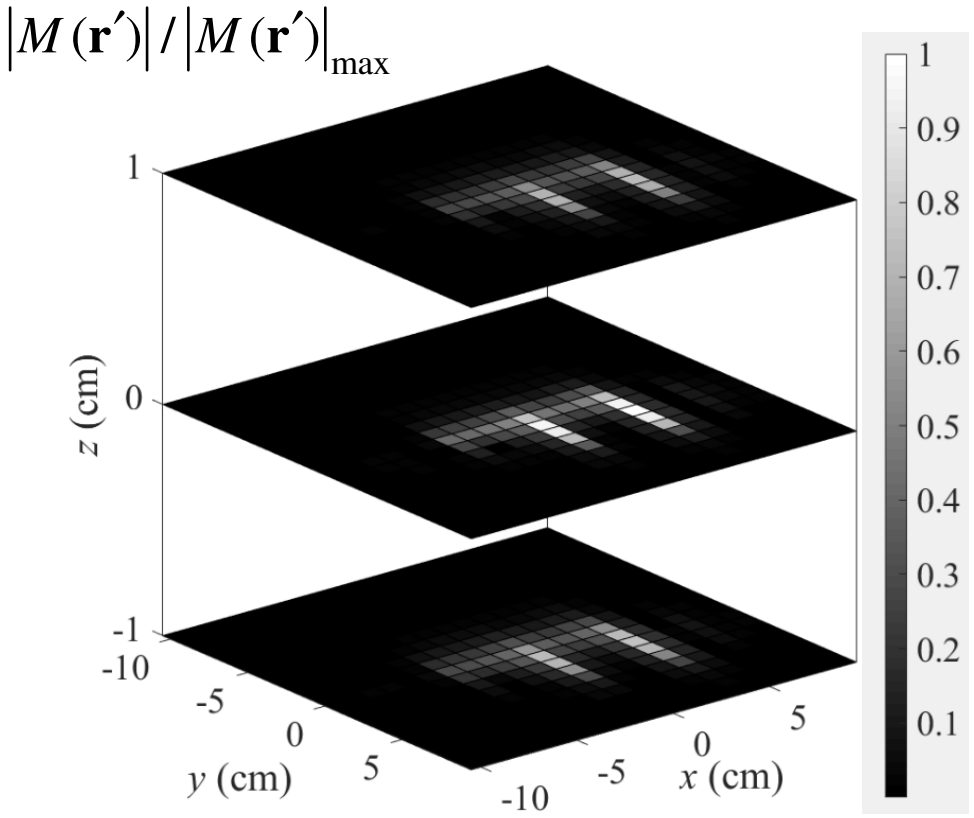

- blurring typical for cross-correlation methods due to
  - ➢ limited sampling
  - ➢ limited viewing angle (aperture size)

We can do better with SPM Stage 2 with the same data!

SPM STAGE 2: QUANTITATIVE IMAGING AND IMPROVED RESOLUTION

[Tu *et al.*, *Inverse Problems* 2015]][Nikolova, *Introduction to Microwave Imaging*, 2017]

- SPM Stage 2 processes the OUT power map to ***improve image spatial resolution*** and to reveal the ***quantitative contrast*** information embedded in the OUT power map $M(\mathbf{r}')$
- solves

$$M(\mathbf{r}') = \frac{1}{\Delta\varepsilon_{\mathrm{r,sp}}\Omega_{\mathrm{sp}}} \iiint_{V_\mathrm{s}} \Delta\varepsilon_\mathrm{r}(\mathbf{r}'')\, \underbrace{M^{H}_{\mathrm{sp}@\mathbf{r}''}(\mathbf{r}')}_{\text{SP scattered power map}} d\mathbf{r}''$$

$$M^{H}_{\mathrm{sp}@\mathbf{r}''}(\mathbf{r}') = \sum_{\zeta=1}^{N_\mathrm{T}} \int_\omega \iint_{S_\mathrm{a}} \underbrace{H^{\mathrm{sc}}_\zeta(\mathbf{r}-\mathbf{r}'',\omega)}_{\text{SP data}} \Big[\underbrace{H^{\mathrm{sc}}_\zeta(\mathbf{r}-\mathbf{r}',\omega)}_{\text{PSF}}\Big]^* d\mathbf{r}\, d\omega$$

  - SP power maps obtained just like OUT power map

- power maps (OUT and SP) are on uniform grid → *kz*-space inversion for the permittivity contrast provides the best computational speed

SPM STAGE 2: SCATTERING-PROBE (SP) POWER MAPS

- in addition to the OUT power map $M(\mathbf{r}')$, Stage 2 needs SP power maps $M^{H}_{\mathrm{sp}@\mathbf{r}''}(\mathbf{r}')$ for a SP at each voxel position: $\forall \mathbf{r}'' \in V_s$
- BUT with uniform background, SP power maps are translationally invariant in the lateral directions, e.g., in planar scanning

$$M^{H}_{\mathrm{sp}@(x'',y'',z'')}(x',y',z') = M^{H}_{\mathrm{sp}@(0,0,z'')}(x'-x'',y'-y'',z')$$

SP at center of image slice at z''

$$\Rightarrow \quad M(x',y',z') = \frac{1}{\Delta\varepsilon_{\mathrm{r,sp}}\Omega_{\mathrm{sp}}} \int_{z''}\int_{y''}\int_{x''} \Delta\varepsilon_{\mathrm{r}}(x'',y'',z'') M^{H}_{\mathrm{sp}@(0,0,z'')}(x'-x'',y'-y'',z')\,dx''dy''dz''$$

2D convolution

$$\Downarrow$$

Stage 2 in *kz* space: $$\tilde{M}(k_x,k_y,z') = \frac{\Delta x'\Delta y'}{\Delta\varepsilon_{\mathrm{r,sp}}\Omega_{\mathrm{sp}}} \int_{z''} \Delta\tilde{\varepsilon}_{\mathrm{r}}(k_x,k_y,z'') \tilde{M}^{H}_{\mathrm{sp}@z''}(k_x,k_y,z')\,dz''$$

- we need only the power maps for SP in the center of each imaged slice at z'' (N_z 3D maps)

$$\tilde{M}^{H}_{\mathrm{sp}@z''_q}(k_x,k_y,z'_p),\ p,q=1,\ldots,N_z$$

SPM STAGE 2: SCATTERING-PROBE (SP) POWER MAPS

- SP power maps are computed just like the OUT power map, only with the data from the SP measurement

SP power maps in (x', y', z') space:

$$M^{H}_{\mathrm{sp}@(0,0,z'')}(x', y', z') = \sum_{\zeta=1}^{N_\mathrm{T}} \int_{\omega} \underbrace{\iint_{S_\mathrm{a}} H^{\mathrm{sc}}_{\zeta}(x, y, \overline{z}, \omega; z'') \left[H^{\mathrm{sc}}_{\zeta}(x - x', y - y', \overline{z}, \omega; z') \right]^{*} dx dy}_{\text{2D convolution}} \, d\omega$$

SP power maps in (k_x, k_y, z') space:

$$\tilde{M}^{H}_{\mathrm{sp}@z''}(k_x, k_y, z') = \sum_{\zeta=1}^{N_\mathrm{T}} \sum_{k=1}^{N_\omega} \left[\tilde{H}_{\zeta}(k_x, k_y, \overline{z}, \omega_k; z'') \right] \left[\tilde{H}_{\zeta}(k_x, k_y, \overline{z}, \omega_k; z') \right]^{*}$$

SPM STAGE 2 IMPLEMENTATION

[R. Kazemivala *et al.*, *IEEE Trans. MTT*, 2022]

Stage 2: image deconvolution and quantitative reconstruction

$$\tilde{M}(k_x,k_y,z') = \frac{\Delta x'\Delta y'}{\Delta\varepsilon_{\mathrm{r,sp}}\Omega_{\mathrm{sp}}}\int_{z''}\Delta\tilde{\varepsilon}_{\mathrm{r}}(k_x,k_y,z'')\tilde{M}^{H}_{\mathrm{sp}@z''}(k_x,k_y,z')\,dz''$$

⇩ *discretize integral*

$$\tilde{M}(\boldsymbol{\kappa}_{ij},z'_q) = \frac{\overbrace{\Delta x'\Delta y'\Delta z'}^{\Omega_{\mathrm{v}}}}{\Delta\varepsilon_{\mathrm{r,sp}}\Omega_{\mathrm{sp}}}\sum_{p=1}^{N_z}\Delta\tilde{\varepsilon}_{\mathrm{r}}(\boldsymbol{\kappa}_{ij},z''_p)\,\tilde{M}^{H}_{\mathrm{sp}@z''_p}(\boldsymbol{\kappa}_{ij},z'_q)$$

imaged voxel range position — *scatterer range position*

$$\boldsymbol{\kappa}_{ij} = (i\Delta k_x,\, j\Delta k_y)$$
$$i = 1,\ldots,N_x$$
$$j = 1,\ldots,N_y$$
$$q = 1,\ldots,N_z$$

- $N_z \times N_z$ system of equations solved at each point in Fourier space, $\boldsymbol{\kappa}_{ij} = (i\Delta k_x,\, j\Delta k_y)$

$$\boxed{\mathbf{M}(\boldsymbol{\kappa}_{ij})\,\tilde{\boldsymbol{\rho}}(\boldsymbol{\kappa}_{ij}) = \mathbf{m}(\boldsymbol{\kappa}_{ij})}$$

Stage 2 systems of equations in *kz* space

SP@z_1 Stage 1 power map

$$\mathbf{M}(\boldsymbol{\kappa}_{ij})\,\tilde{\boldsymbol{\rho}}(\boldsymbol{\kappa}_{ij}) = \mathbf{m}(\boldsymbol{\kappa}_{ij})$$

$$\mathbf{M}(\boldsymbol{\kappa}_{ij}) = \begin{bmatrix} \tilde{M}_{\mathrm{sp}@z_1}(\boldsymbol{\kappa}_{ij}, z_1) & \cdots & \tilde{M}_{\mathrm{sp}@z_{N_z}}(\boldsymbol{\kappa}_{ij}, z_1) \\ \vdots & \ddots & \vdots \\ \tilde{M}_{\mathrm{sp}@z_1}(\boldsymbol{\kappa}_{ij}, z_{N_z}) & \cdots & \tilde{M}_{\mathrm{sp}@z_{N_z}}(\boldsymbol{\kappa}_{ij}, z_{N_z}) \end{bmatrix}_{N_z \times N_z}$$

OUT Stage 1 power map

$$\mathbf{m}(\boldsymbol{\kappa}_{ij}) = \begin{bmatrix} \tilde{M}(\boldsymbol{\kappa}_{ij}, z_1) \\ \vdots \\ \tilde{M}(\boldsymbol{\kappa}_{ij}, z_{N_z}) \end{bmatrix}$$

$$\tilde{\boldsymbol{\rho}}(\boldsymbol{\kappa}_{ij}) = \frac{\Omega_{\mathrm{v}}}{\Delta\varepsilon_{\mathrm{r,sp}}\Omega_{\mathrm{sp}}} \left[\Delta\tilde{\varepsilon}_{\mathrm{r}}(\boldsymbol{\kappa}_{ij}, z_1) \quad \cdots \quad \Delta\tilde{\varepsilon}_{\mathrm{r}}(\boldsymbol{\kappa}_{ij}, z_{N_z}) \right]^T$$

- final step: back to (*x*,*y*) space

$$\Delta\varepsilon_{\mathrm{r}}(x', y', z'_p) = \frac{\Delta\varepsilon_{\mathrm{r,sp}}\Omega_{\mathrm{sp}}}{\Omega_{\mathrm{v}}} \mathrm{FT}_{\mathrm{2D}}^{-1}\left\{\tilde{\rho}(\boldsymbol{\kappa}; z'_p)\right\},\ p = 1, \ldots, N_z$$

SIMULATION EXAMPLE: SPM STAGE 1 AND STAGE 2 IMAGES OF F-SHAPE

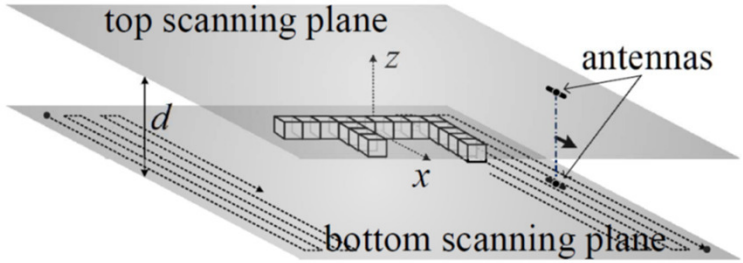

$$\varepsilon_{r,b} = 1.0$$
$$\varepsilon_{r,F} = 1.2 + i0.0$$

Stage 1 qualitative image

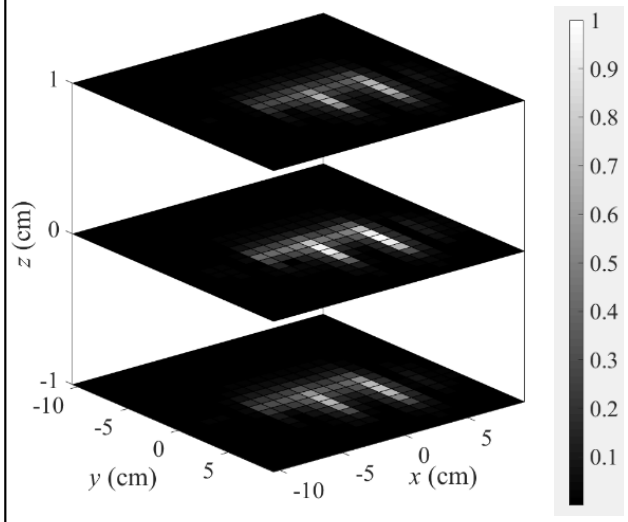

Stage 2 quantitative image

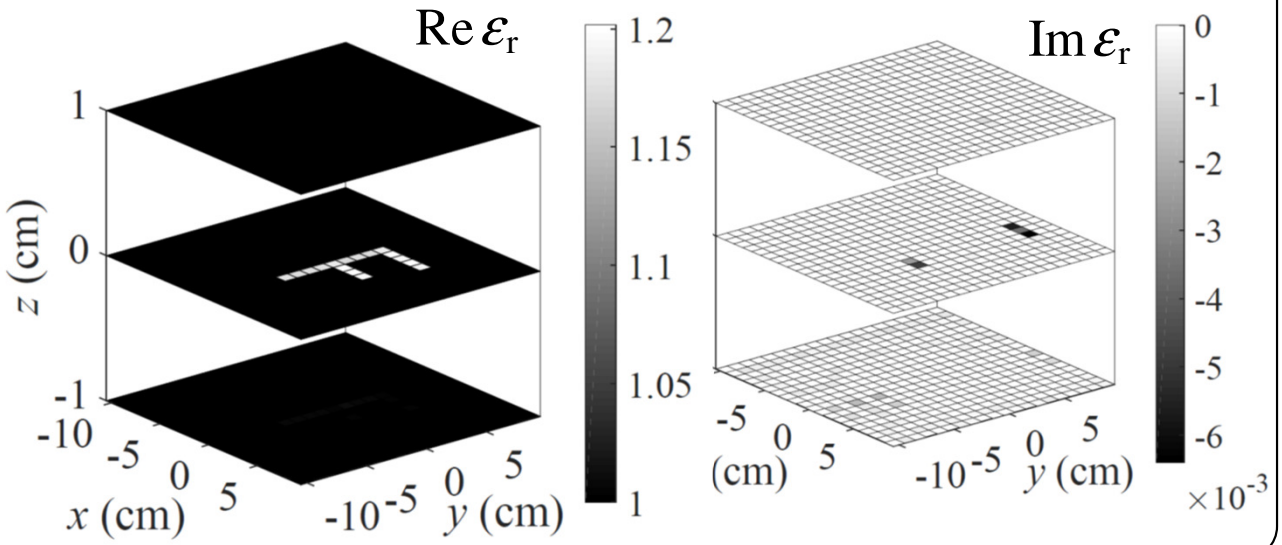

SUMMARY: SCATTERED-POWER MAPPING

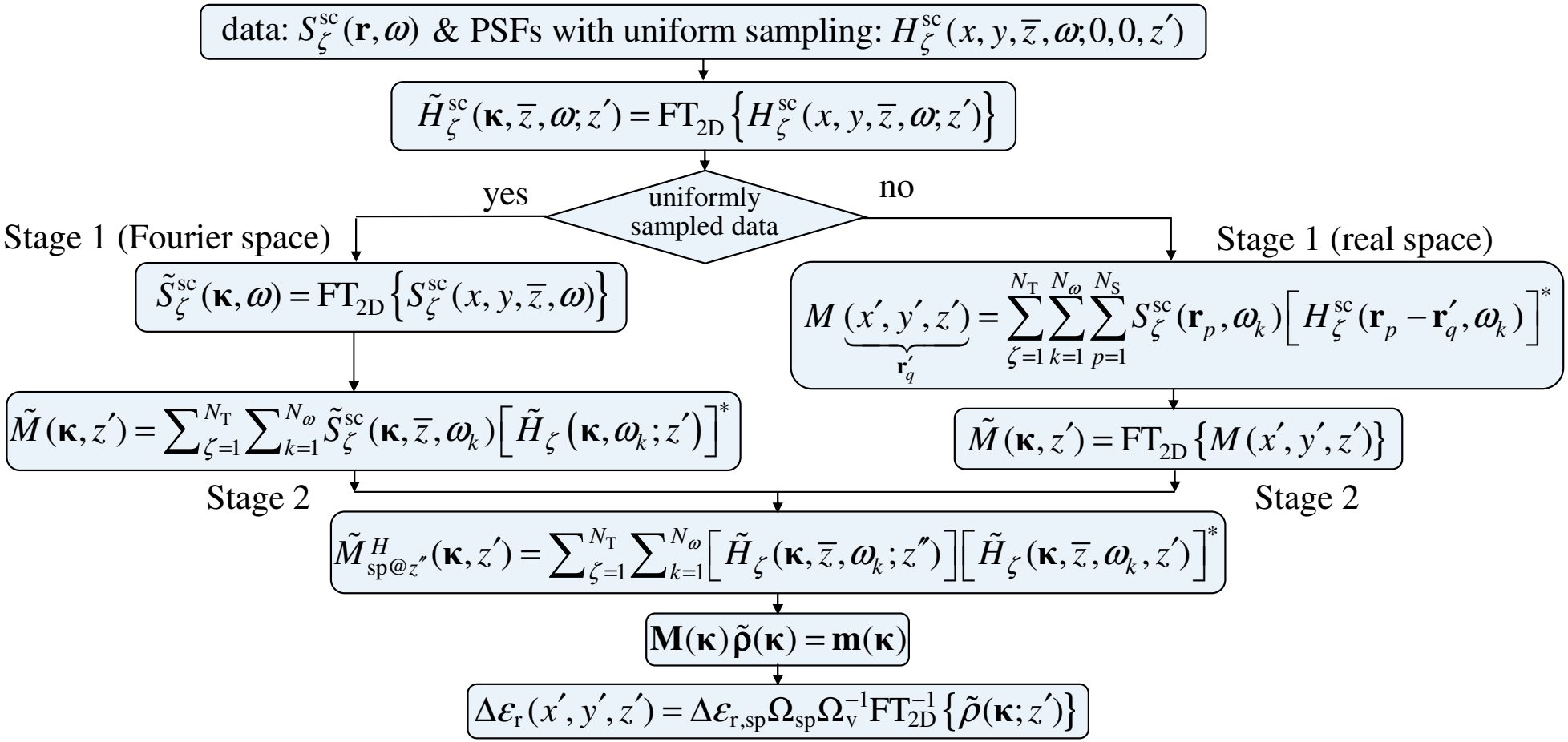

EXAMPLE: SPM IMAGING OF COMPRESSED-BREAST PHANTOM (35 MM)

- mechanical scan, 18×18 cm^2 ($\Delta_{x,y}$ = 3 mm), 3 GHz - 8 GHz SFCW (Δ_f =100 MHz), S_{21}

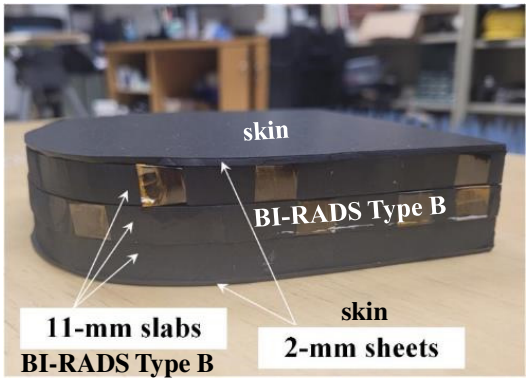

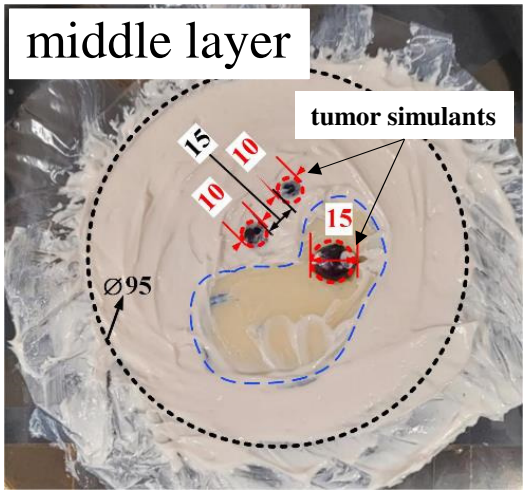

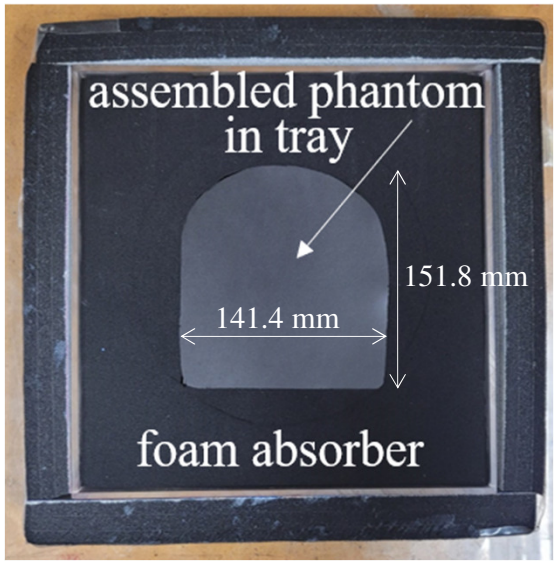

[N. Shahmirzadi *et al.*, *IEEE Trans. AP*, 2023]
[R. Kazemivala *et al.*, *Sensors*, 2024]

projection images of ***complex permittivity***

[image credits: Romina Kazemivala]

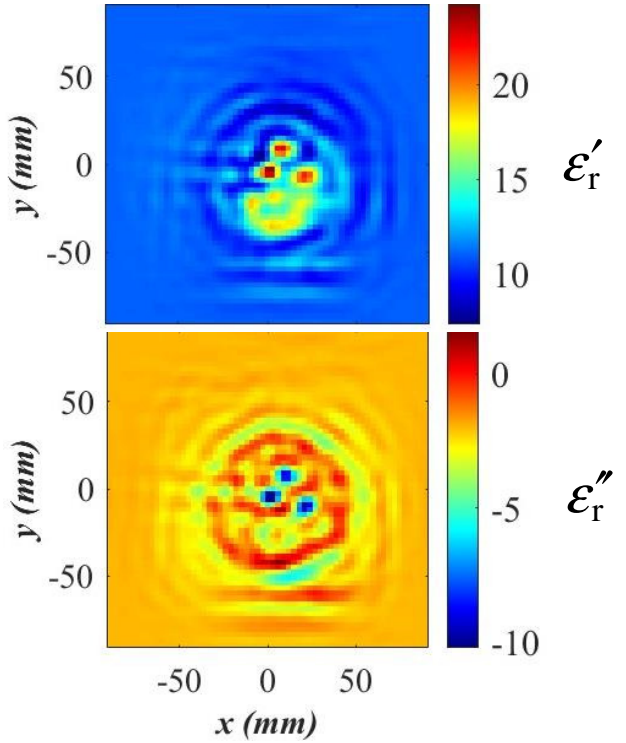

EXAMPLE: SPM mm-WAVE IMAGING WITH SFCW (VNA) DATA

- quantitative images of penetrable objects with spatial resolution ~3 mm (~$\lambda_c/3$)

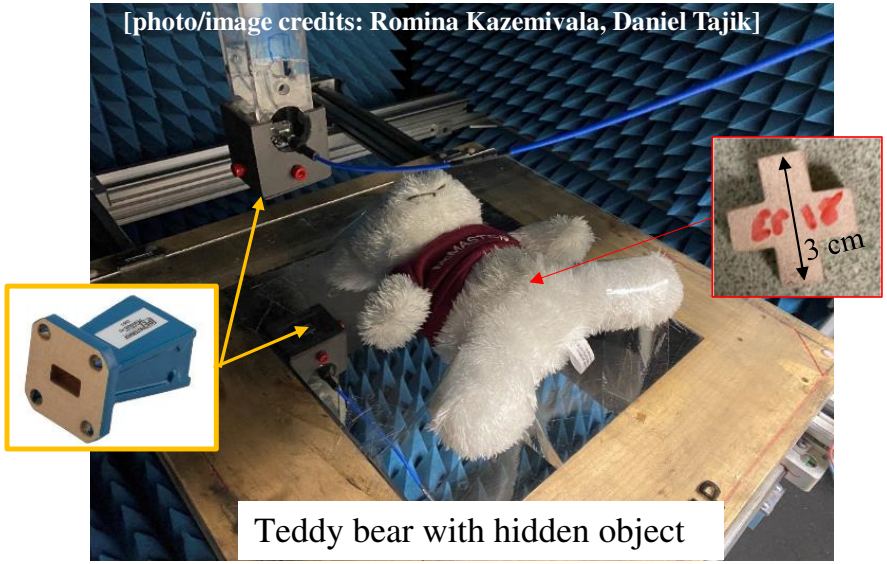

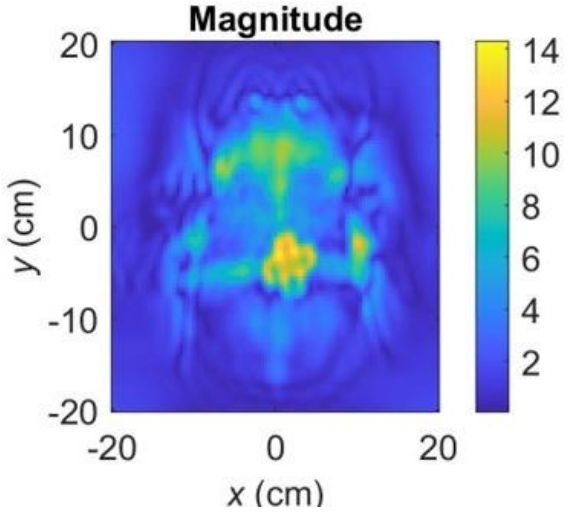

[R. Kazemivala *et al.*, *IEEE Trans. MTT*, 2022]

- mechanical scan, 20×20 cm^2 ($\Delta_{x,y}$ = 2 mm)
- 26 GHz - 40 GHz (Δ_f = 200 MHz)
- WR28 horn antennas
- S_{21} data

EXAMPLES: SPM IMAGING WITH MIMO LFM RADAR

- SPM works with chirp (LFM) radar signals as well

TI mm-Wave Sensor IWR1443
LFM MIMO Radar 79 GHz to 83 GHz
$\lambda_c \approx 3.8$ mm

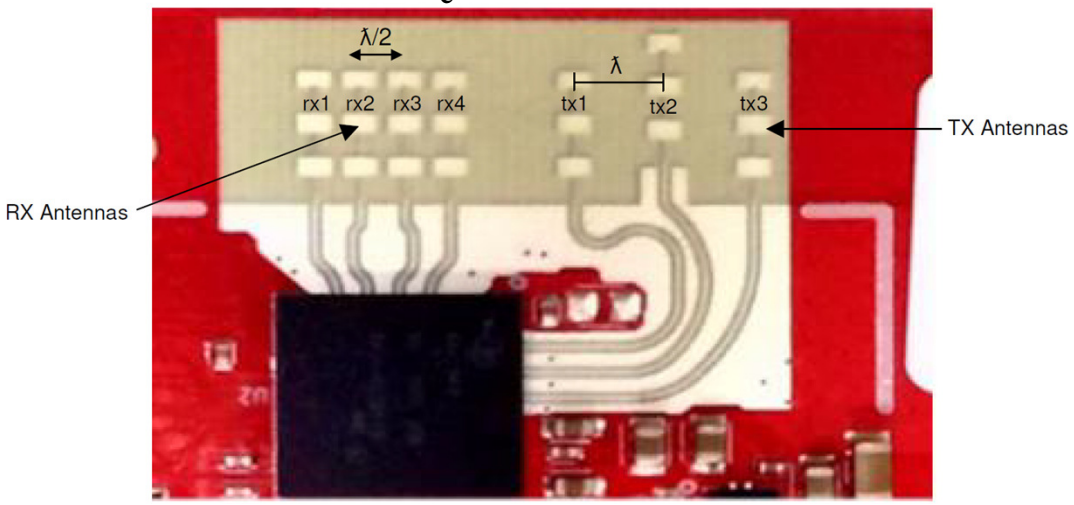

chamber with scanner

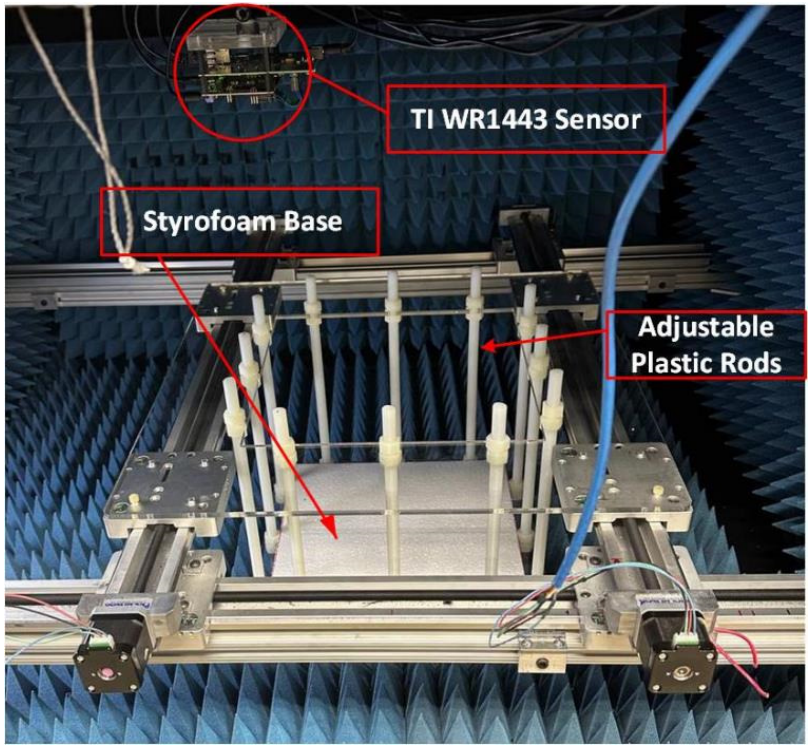

[Kazemivala *et al.*, *IEEE Trans. MTT*, 2024]

EXAMPLES: SPM IMAGING WITH MIMO LFM RADAR, cont.

SPM reflectivity 2D images (qualitative)

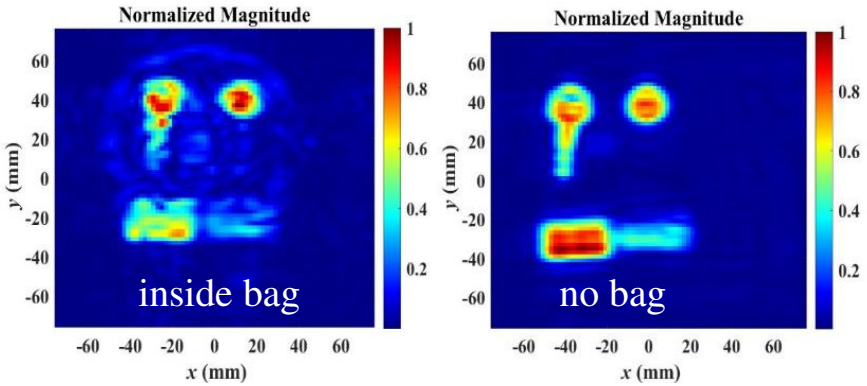

3D imaging (qualitative)

$\overline{z} = 225$ mm

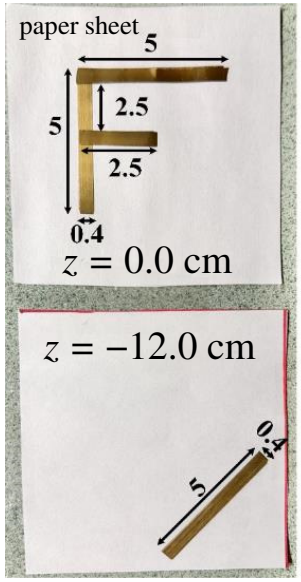

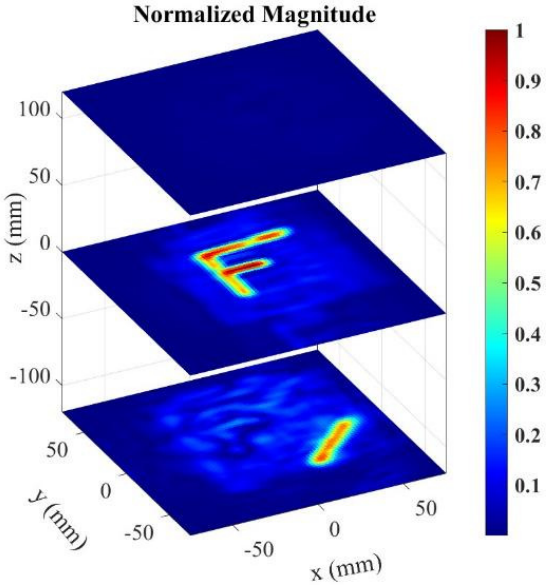

[Kazemivala *et al.*, *IEEE Trans. MTT*, 2024]

FILTERING IN FOURIER SPACE IMAGE RECONSTRUCTION

[Tajik *et al.*, *Progress In Electromagn. Res. B*, 2017]

- there are two main filtering strategies often needed in Fourier-space imaging

BEFORE FFT	BEFORE Inverse FFT
Apodization Filter ➢ operates on data sets, PSFs, SPM Stage 1 power maps in real space, e.g., (x,y) ➢ acts as "window" to suppress edge values	**Low-pass Filter** ➢ operates on computed contrast in Fourier space, e.g., (k_x, k_y) ➢ suppresses high-k components
• circular DFT (FFT) wraps around the left edge of the 2D data set to its right edge and the top edge to the bottom edge • this edge-to-edge transition must be smooth (data edge continuity) • without data edge continuity, Gibb's effect leads to ringing artifacts corrupting computations in k-space	• at high wavenumbers, signal is mostly due to measurement noise (very rapid change in real space) → erroneous contrast values $\tilde{\rho}(\boldsymbol{\kappa}; z_q')$ • 2D LPF suppresses likely erroneous contrast outside the region $\kappa_\xi \geq \kappa_{\xi\max} = \frac{4\pi}{\lambda_{\min}} \sin\alpha,\ \xi = x, y$

C-SHAPE & CUBICLES EXAMPLE: APODIZATION FILTERING

[Tajik *et al.*, *Progress In Electromagn. Res. B*, 2017]

- simulated data (*Altair FEKO*), 3 GHz to 8 GHz with Δ_f = 1 GHz
- $\Delta_x = \Delta_y$ = 1 cm $\approx \lambda_{min}/3$

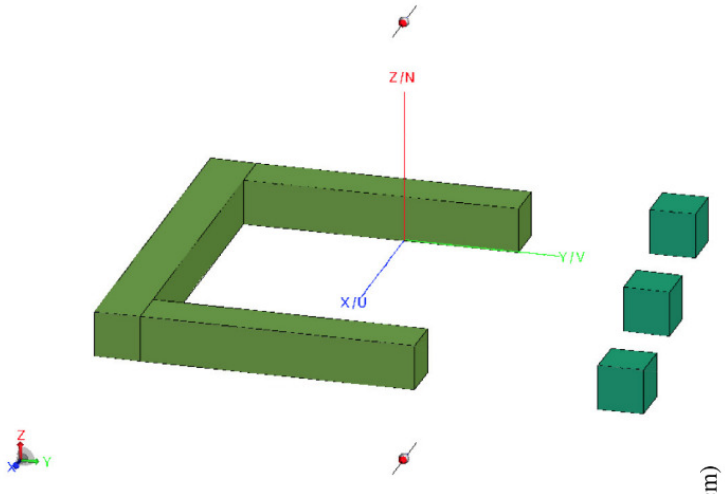

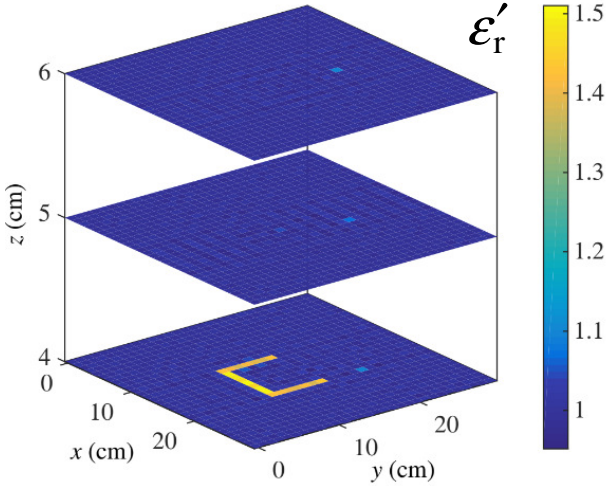

example of scan data (at 8 GHz) with acceptable edge continuity

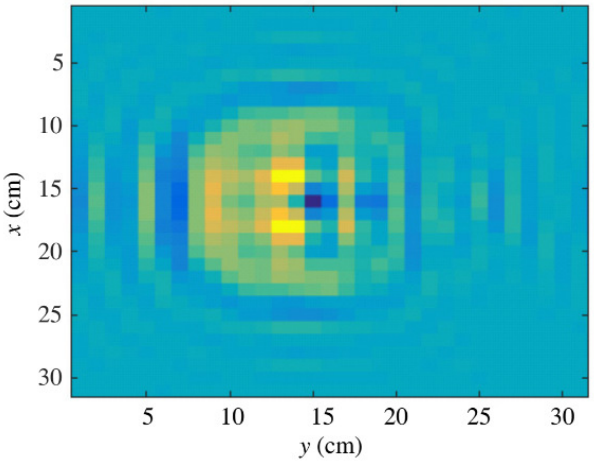

QMH image (no need for data apodization)

C-SHAPE & CUBICLES EXAMPLE: APODIZATION FILTERING, cont.

[Tajik *et al.*, *Progress In Electromagn. Res. B*, 2017]

example of intentionally corrupted scan data (at 8 GHz)

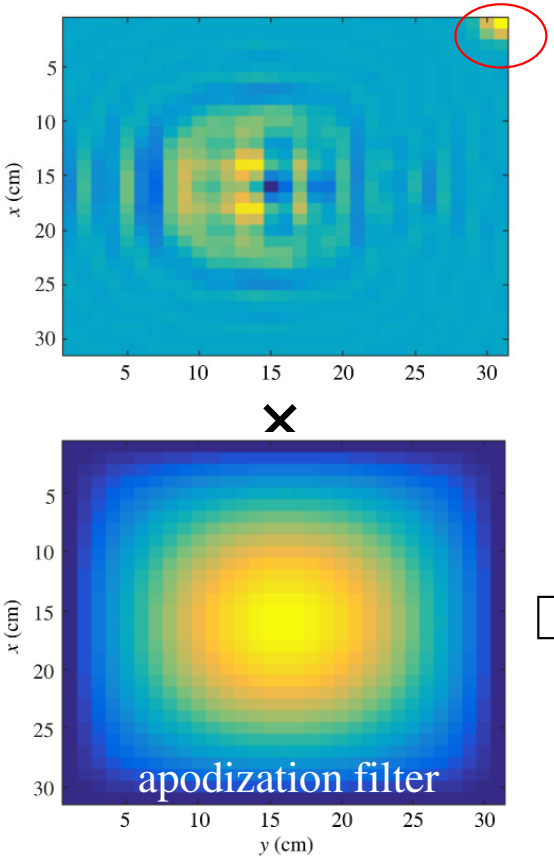

QMH image without data apodization

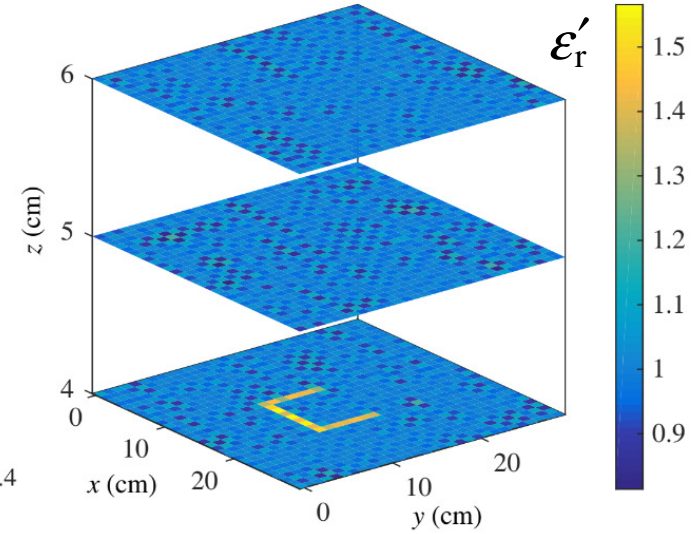

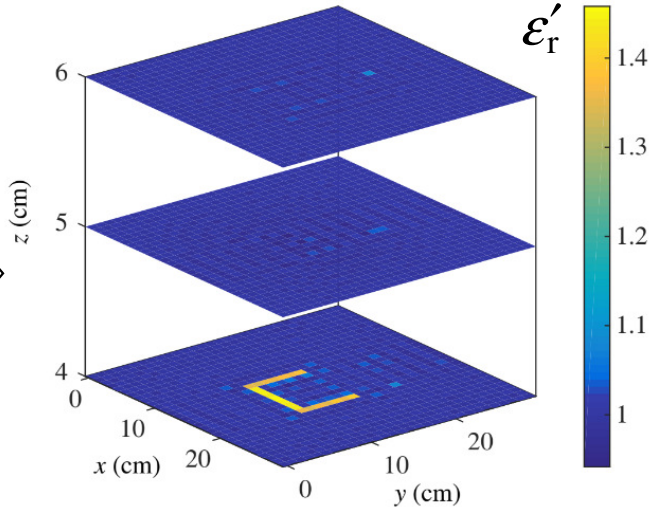

QMH image with data apodization

C-SHAPE & CUBICLES EXAMPLE: LOW-PASS FILTERING

[Tajik *et al.*, *Progress In Electromagn. Res. B*, 2017]

- original spatial sampling of $\Delta_x = \Delta_y = 1$ cm $\approx \lambda_{\min}/3$

$$\Rightarrow \kappa_\xi < \kappa_{\xi\max} = \frac{4\pi}{\lambda_{\min}} \sin\alpha \text{ for } \forall \kappa_\xi,\ \xi = x, y$$

QMH quantitative image (no need for LPF)

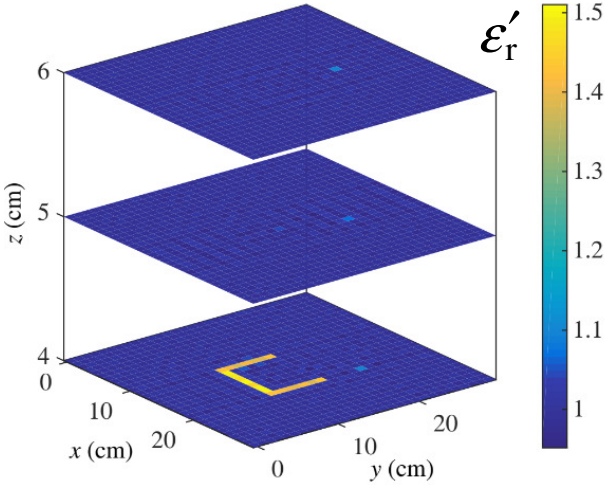

- intentional over-sampling of $\Delta_x = \Delta_y = 0.5$ cm $\approx \lambda_{\min}/8$

$$\Rightarrow \sup|\kappa_\xi| > \kappa_{\xi\max},\ \xi = x, y$$

QMH image from over-sampled data (no LPF)

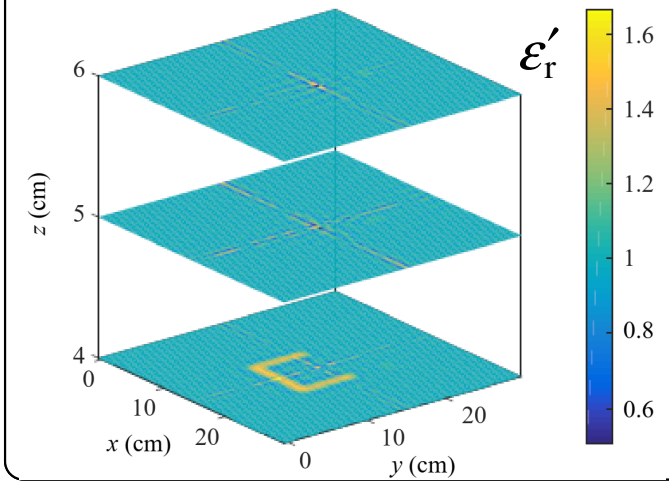

QMH image from over-sampled data (with LPF)

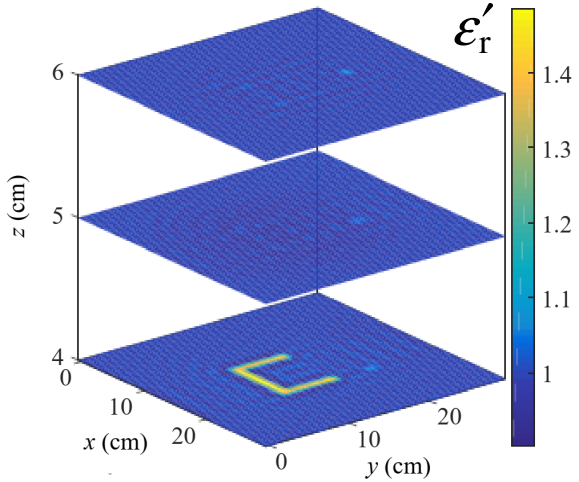

SUMMARY OF PART 3

- the data PSFs give the kernels of the data equations (for all response types and frequencies) and are thus at the core of all direct (linear) image-reconstruction methods
- measured PSFs with scattering probes of known permittivity and volume enables quantitative imaging with fast direct image reconstruction
- QMH solves directly the linearized data equation in *kz* space
- SPM Stage 1 forms the object's projection image (OUT power map) and then Stage 2 deconvolves (in *kz* space) this image with the images of point scatterers (SP power maps) at each imaged range slice
- the computational speeds of QMH and SPM are comparable when SPM Stage 1 is performed in Fourier (*kz*) space
- *kz*-space image reconstruction with QMH and SPM Stage 1 requires uniform spatial sampling to take advantage of fast Fourier transform (forward and inverse)
- real-space image reconstruction with SPM Stage 1 is slower but it can process randomly sampled data on the run → suitable for vehicle-borne radars

SUMMARY OF PART 3, cont.

- filtering is often required with measured data
- apodization ensures edge continuity across an aperture
- low-pass filtering helps suppress erroneously reconstructed contrast at high spatial frequencies

QUESTIONS?

CONCLUDING REMARKS: OUTLOOK TO THE FUTURE

- MMW imaging and sensing – the new frontier of wireless technology
- **main hardware challenge**: accelerating measurements with electronically switched antenna arrays and Tx/Rx electronics
  - ➢ the first real-time MMW whole-body scanners have recently become available for security inspection of walking people and industrial inspection of goods
  - ➢ progress is slower in biomedical imagers
- new and improved image reconstruction algorithms
  - ➢ sparse and random 3D sampling for handheld and mobile/UAV platforms
- new technologies: **sub-THz imaging** (300 GHz to 1 THz)
  - ➢ imaging with incoherent (magnitude only) data
  - ➢ spectroscopic imaging – quantitative images as a function of frequency?

qualitative → quantitative → spectroscopic

reflectivity $0 \le \rho \le 1$ $(\varepsilon', \varepsilon'')$ $\varepsilon'(\omega), \varepsilon''(\omega)$

THANK YOU!

REFERENCES

Kazemivala *et al*., "Real-time millimeter-wave imaging with linear frequency modulation radar and scattered power mapping," *IEEE Trans. Microwave Theory Tech.*, vol. 72, 2024.

Amineh *et al*., "Three-dimensional near-field microwave holography for tissue imaging," *Int. J. of Biomedical Imaging*, vol. 2012, 2012.

Amineh *et al*., "Microwave holography using measured point-spread functions," *IEEE Trans. Instrum.&Meas.*, vol. 64, 2015.

Tajik *et al*., "Quality control of microwave equipment for tissue imaging," *IEEE J. Electromagnetics, RF, and Microwaves in Medicine and Biology (J-ERM)*, vol. 4, 2020.

Tajik *et al*., "Real-time imaging with simultaneous use of Born and Rytov approximations in quantitative microwave holography," *IEEE Trans. Microwave Theory Tech.*, vol. 70, 2022.

Tajik *et al*., "Accurate range migration for fast quantitative Fourier-based image reconstruction with monostatic radar," *IEEE Trans. Microwave Theory Tech*., vol. 70, 2022.

Sheng Tu *et al*., "Fast quantitative microwave imaging with resolvent kernel extracted from measurements," *Inverse Problems*, vol. 31, 2015.

Shumakov *et al*., "Fast quantitative microwave imaging with scattered-power maps," *IEEE Trans. Microwave Theory Tech*., vol. 66, 2018.

Nikolova, *Introduction to Microwave Imaging*. Cambridge University Press, 2017.

Kazemivala *et al*., "Simultaneous use of the Born and Rytov approximations in real-time imaging with Fourier-space scattered power mapping," *IEEE Trans. Microwave Theory Tech.*, vol. 70, 2022.

Shahmirzadi *et al*., "Planar array of UWB active slot antennas for microwave imaging of the breast," *IEEE Trans. Antennas Propagat.*, vol. 71, 2023.

Kazemivala *et al*., "Real-time synthetic aperture radar imaging with random sampling employing scattered power mapping," *Sensors*, vol. 24, 2024.

Tajik *et al.*, "Comparative study of the Rytov and Born approximations in quantitative microwave holography," *Progress in Electromagn. Res. B*, vol. 79, 2017.

EXAMPLE: SPM IMAGING OF MULTILAYER SAMPLE FOR NDT

[Shumakov *et al.*, *IEEE Trans. MTT*, 2018]

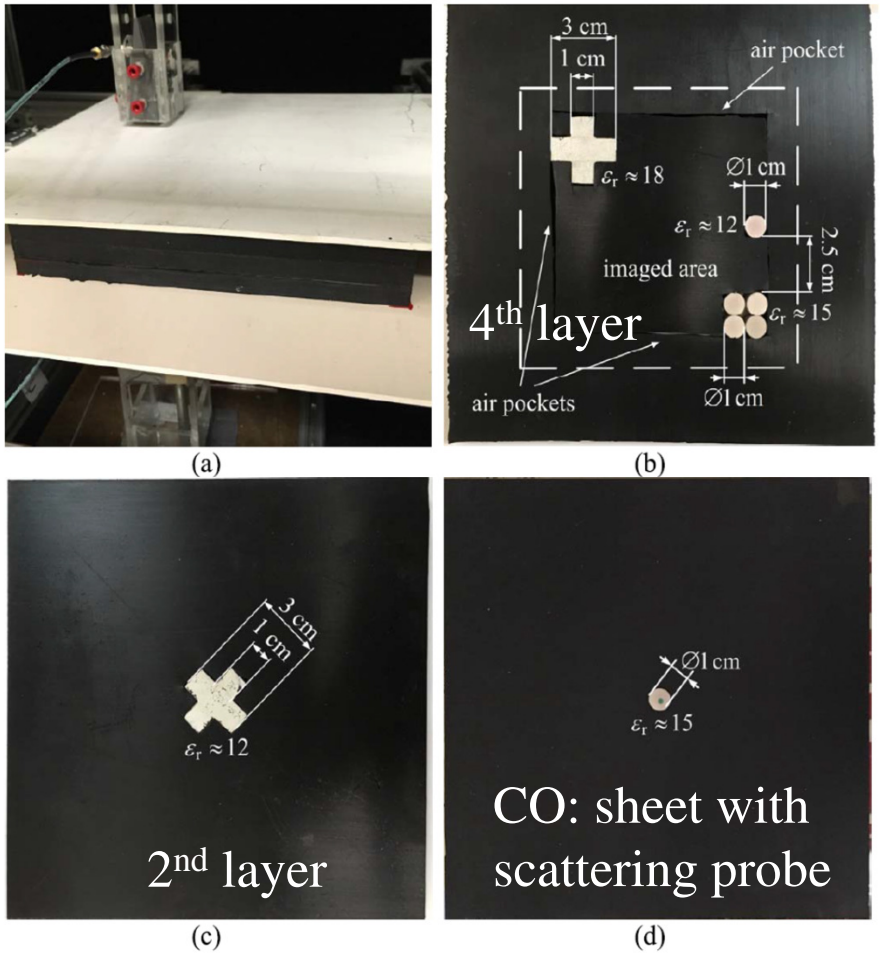

- 5 cm thick carbon-rubber sample $\varepsilon_{r,b} \approx 10 - i5$
- frequency: from 3 GHz to 9 GHz (61 samples)
- scattering probe $\varepsilon_{r,sp} \approx 15 - i0.003$
- all embedded objects are 1 cm thick
- reflection and transmission coefficients on two TEM horn antennas aligned along boresight
- imaged area 13 cm by 13 cm (2 mm sampling step)

EXAMPLE: SPM IMAGING OF MULTILAYER SAMPLE FOR NDT, cont.

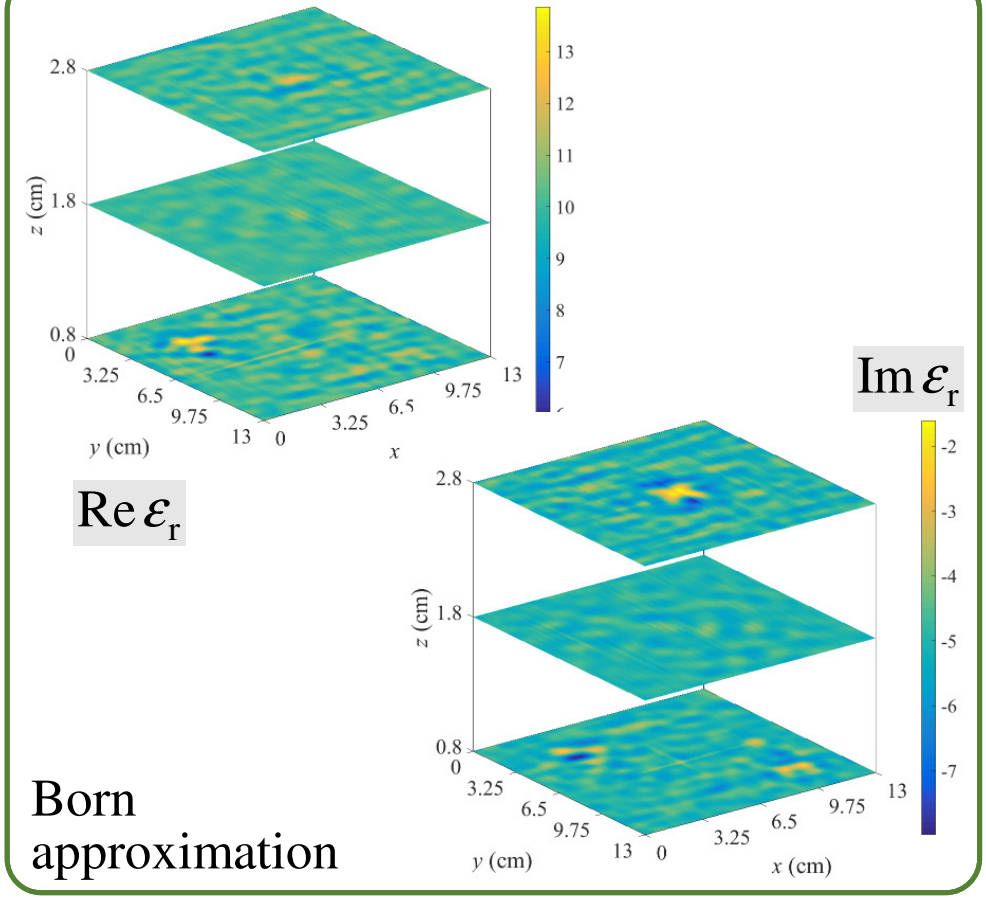

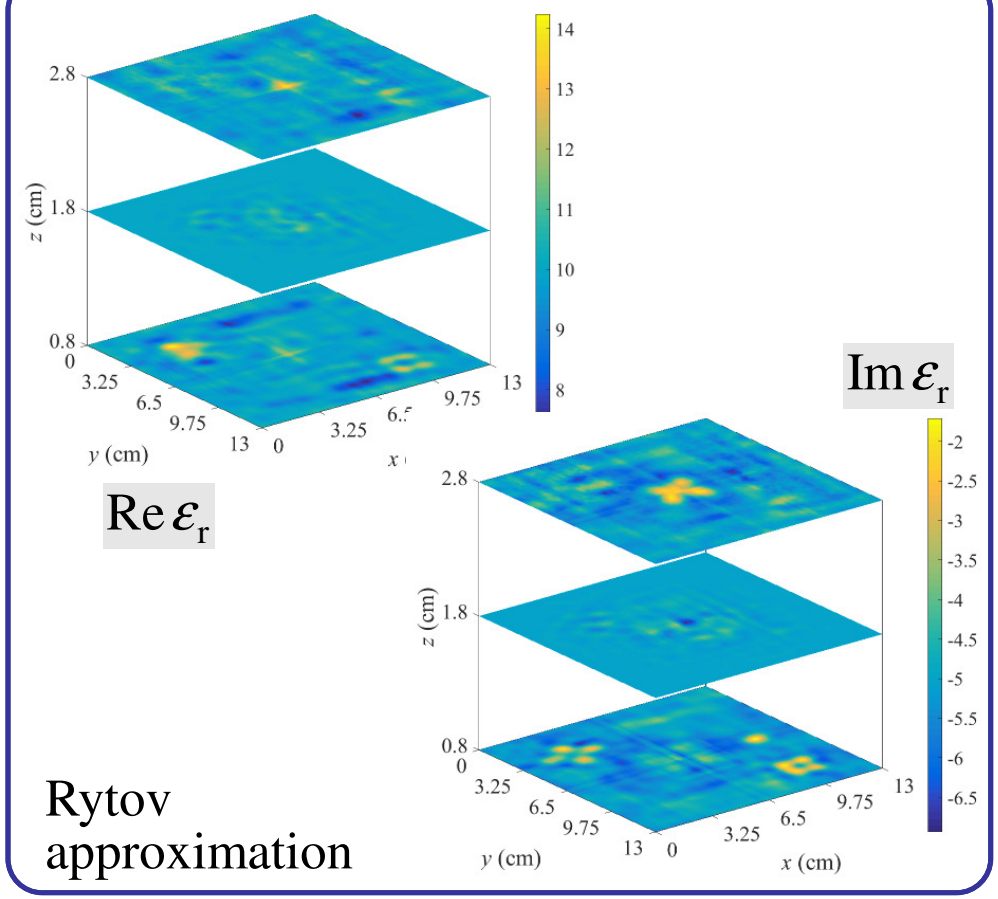

[Shumakov *et al.*, *IEEE Trans. MTT*, 2018]